High-performing neural network models of visual cortex benefit from high latent dimensionality

Eric Elmoznino[*]
Department of Cognitive Science
Johns Hopkins University
Baltimore, MD 21218
eric.elmoznino@gmail.com

Michael F. Bonner
Department of Cognitive Science
Johns Hopkins University
Baltimore, MD 21218
mfbonner@jhu.edu

Abstract

Geometric descriptions of deep neural networks (DNNs) have the potential to uncover core principles of computational models in neuroscience, while abstracting over the details of model architectures and training paradigms. Here we examined the geometry of DNN models of visual cortex by quantifying the latent dimensionality of their natural image representations. A popular view holds that optimal DNNs compress their representations onto low-dimensional subspaces to achieve invariance and robustness, which suggests that better models of visual cortex should have low-dimensional geometries. Surprisingly, we found a strong trend in the opposite direction—neural networks with high-dimensional image subspaces tend to have better generalization performance when predicting cortical responses to held-out stimuli in both monkey electrophysiology and human fMRI data. These findings held across a diversity of design parameters for DNNs, and they suggest a general principle whereby high-dimensional geometry confers a striking benefit to DNN models of visual cortex.

1 Introduction

Deep neural networks (DNNs) are the predominant framework for computational modeling in neuroscience (Hassabis, Kumaran, Summerfield, & Botvinick, 2017; Kriegeskorte, 2015; Lindsay, 2020; Richards et al., 2019; Yamins & DiCarlo, 2016). When using DNNs to model neural systems, one of the fundamental questions that researchers hope to answer is: What core factors explain why some DNNs succeed and others fail? Researchers often attribute the success of DNNs to explicit design choices in a model's construction, such as its architecture, learning objective, and training data (Cadena et al., 2022; Cao & Yamins, 2021a, 2021b; Conwell, Prince, Alvarez, & Konkle, 2022; Dwivedi, Bonner, Cichy, & Roig, 2021; Khaligh-Razavi & Kriegeskorte, 2014; Konkle & Alvarez, 2022; Kriegeskorte, 2015; Lindsay, 2020; Yamins & DiCarlo, 2016; Yamins et al., 2014; Zhuang et al., 2021). However, an alternative perspective explains DNNs through the geometry of their latent representational subspaces, which abstracts over the details of training procedures and architectures (Chung & Abbott, 2021; Chung, Lee, & Sompolinsky, 2018; Cohen, Chung, Lee, & Sompolinsky, 2020; Jazayeri & Ostojic, 2021; Sorscher, Ganguli, & Sompolinsky, 2021). Here we sought to understand the geometric principles that underlie the performance of DNN models of visual cortex.

We examined the geometry of DNNs by quantifying the dimensionality of their representational subspaces. DNN models of vision contain thousands of artificial neurons, but their representations are known to be constrained to lower-dimensional subspaces that are embedded within the ambient space of the neural population (e.g. Ansuini, Laio, Macke, & Zoccolan, 2019). Many have argued that DNNs benefit from representing stimuli in subspaces that are as low-dimensional as possible

[*]Corresponding author.

Preprint. Under review.

(either at local scales, global scales, or both), and it is proposed that low dimensionality improves a network's generalization performance, its robustness to noise, and its ability to separate stimuli into meaningful categories (Amsaleg et al., 2017; Ansuini et al., 2019; Feng et al., 2022; I. Fischer & Alemi, 2020; I. S. Fischer, 2020; Gong, Boddeti, & Jain, 2019; Kingma & Welling, 2013; Lee, Arnab, Guadarrama, Canny, & Fischer, 2021; Ma et al., 2018; Pope, Zhu, Abdelkader, Goldblum, & Goldstein, 2021; Recanatesi et al., 2019; Tishby & Zaslavsky, 2015; Zhu et al., 2018). Similar arguments have been made for the benefits of low-dimensional subspaces in the sensory, motor, and cognitive systems of the brain (Churchland et al., 2012; Gallego, Perich, Miller, & Solla, 2017; Gao & Ganguli, 2015; Lehky, Kiani, Esteky, & Tanaka, 2014; Nieh et al., 2021; Op de Beeck, Wagemans, & Vogels, 2001; Saxena & Cunningham, 2019). However, contrary to this view, there are also potential benefits of high-dimensional subspaces, including the efficient utilization of a network's representational resources and increased expressivity, making for a greater number of potential linear readouts (Barlow, 1961; Fusi, Miller, & Rigotti, 2016; Laakom, Raitoharju, Iosifidis, & Gabbouj, 2021; Olshausen & Field, 1996; Simoncelli & Olshausen, 2001; Stringer, Pachitariu, Steinmetz, Carandini, & Harris, 2019).

We wondered whether the dimensionality of representational subspaces might be relevant for understanding the relationship between DNNs and visual cortex and, if so, what level of dimensionality performs best. To answer these questions, we measured the latent dimensionality of DNNs trained on a variety of supervised and self-supervised tasks using multiple datasets, and we assessed their accuracy at predicting image-evoked activity patterns in visual cortex for held-out stimuli using both monkey electrophysiology and human fMRI data. We discovered a powerful relationship between dimensionality and accuracy: specifically, we found that DNNs with higher latent dimensionality perform better as computational models of visual cortex. This was true even when perfectly controlling for model architecture and the number of parameters in each network, and it could not be explained by overfitting because our analyses explicitly tested each network's ability to generalize to held-out stimuli. Furthermore, we found that high dimensionality also conferred computational benefits when learning to classify new categories of stimuli, providing support for its adaptive role in visual behaviors. Together, these findings suggest that high-performing computational models of visual cortex are characterized by high-dimensional representational subspaces, allowing them to efficiently express a greater diversity of linear readouts for natural images.

2 Results

2.1 Dimensionality and alignment in computational brain models

We set out to answer two fundamental questions about the geometry of DNNs in computational neuroscience. First, is there a relationship between latent dimensionality and DNN performance that generalizes across the architectural and training factors that have typically been emphasized in previous work? Second, if latent dimensionality is indeed related to DNN performance, what level of dimensionality is better? In other words, do DNN models of neural systems primarily benefit from the robustness and invariance of low-dimensional codes or the expressivity of high-dimensional codes? To explore the theoretical issues underlying these questions, we first performed simulations that illustrate how the geometry of latent subspaces influences the ability of representational models to account for variance in brain activity patterns.

For our simulations, we considered a scenario in which all brain representations and all relevant computational models are sampled from a large subspace of image representations called the *natural image subspace*. Here, we use the term subspace to describe the lower-dimensional subspace spanned by the major principal components of a system with higher ambient dimensionality (e.g., neurons). We sampled observations from this natural image subspace and projected these observations onto the dimensions spanned by two smaller subspaces called the *ecological subspace* and the *model subspace*. Projections onto the ecological subspace simulate image representations in the brain, and projections onto the model subspace simulate image representations in a computational model. We analyzed these simulated data using a standard approach in computational neuroscience, known as the encoding-model approach. Specifically, we mapped model representations to brain representations using cross-validated linear regression. This analysis yielded an encoding score, which is the explained variance for held-out data in the cross-validated regression procedure. Computational models with higher encoding scores have better performance when predicting brain representations

for held-out data. Further details regarding the theoretical grounding and technical implementation of our simulations are provided in Appendices B and C.

Using this simulation framework, we can now illustrate how two important factors are related to the performance of computational brain models: effective dimensionality and alignment pressure. *Effective dimensionality* (ED) is a continuous measurement of the number of principal components needed to explain most of the variance in a dataset, and it is a way of estimating *latent* dimensionality in our analyses (see Figure 1a). A model with low ED encodes a relatively small number of dimensions whose variance is larger than the variance attributed to noise (i.e., whose signal-to-noise ratio (SNR) is high). In contrast, a model with high ED encodes many dimensions with high SNR. *Alignment pressure* (AP) quantifies the probability that the high SNR dimensions from a pair of subspaces will be aligned, as depicted in Figure 1b. For example, if the AP between a model subspace and the ecological subspace is high, it means that the model is likely to encode the same dimensions of image representation as those observed in the brain.

Nearly all representational modeling efforts in computational neuroscience seek to optimize AP. For example, when researchers construct models through deep learning or by specifying computational algorithms, the hope is that the resulting model will encode representational dimensions that are strongly aligned with the representations of a targeted brain system. However, if one allows for linear transformations when mapping computational models to brain systems—a procedure that may, in fact, be necessary for evaluating such models (Cao & Yamins, 2021a)—then there are possible scenarios in which model performance can be primarily governed by ED.

To understand how ED can influence model performance, it is helpful to first consider two extreme cases. At one extreme, models with an ED of 1 can explain, at best, a single dimension of brain representation and can only do so when AP is extremely high. Such a model would need to encode a dimension that was *just right* to explain variance in a targeted brain system. At the other extreme, a model with very high ED could potentially explain many dimensions of brain representation and could do so with weaker demands on AP. This means that models with extremely high ED have a higher probability of performing well and need only be partially aligned with a targeted brain system.

The relative contributions of ED and AP will depend on their empirical distribution in actual computational models trained to predict real neural data. To better anticipate the possible outcomes, we varied our simulation parameters and identified distinct regimes for the relationship between ED, AP, and the performance of computational brain models (Figure 1c).

In the *Alignment regime*, the ED of computational models varies significantly less than their AP, such that AP predominantly drives performance in predicting neural activity. This perspective implicitly underlies most deep learning approaches for modeling visual cortex, which emphasize factors affecting the alignment between a model and the brain, such as architecture, layer depth, learning objective, and training images (e.g. Cadena et al., 2022; Cao & Yamins, 2021a, 2021b; Conwell et al., 2022; Dwivedi et al., 2021; Khaligh-Razavi & Kriegeskorte, 2014; Konkle & Alvarez, 2022; Kriegeskorte, 2015; Lindsay, 2020; Yamins & DiCarlo, 2016; Yamins et al., 2014; Zhuang et al., 2021). The alignment-based perspective does not entail any specific predictions about ED and, thus, suggests the null hypothesis that ED and encoding scores are unrelated (Figure 1c left panel).

Alternatively, models might inhabit a *Joint regime* where ED and AP are entangled, such that there exists some optimal dimensionality at which model representations are more likely to be aligned with the brain. Previous work has proposed that both biological and artificial vision systems gain computational benefits by representing stimuli in low-dimensional subspaces (Ansuini et al., 2019; Cohen et al., 2020; Lehky et al., 2014). For instance, it has been hypothesized that dimensionality reduction along the visual hierarchy confers robustness to incidental image features (Amsaleg et al., 2017; Feng et al., 2022; I. Fischer & Alemi, 2020; I. S. Fischer, 2020; Lee et al., 2021; Ma et al., 2018; Recanatesi et al., 2019). This dimensionality-reduction hypothesis implicitly underlies a wide variety of machine learning methods that attempt to encode complex stimuli using a small set of highly informative dimensions (e.g., autoencoders) (Kingma & Welling, 2013; Tishby & Zaslavsky, 2015; Zhu et al., 2018). The strongest version of the low-dimensionality perspective predicts that ED and encoding scores will be negatively correlated or exhibit an inverted U-shape, since models with relatively low-dimensional subspaces would tend to be better aligned with the representations of visual cortex (Figure 1c middle panels).

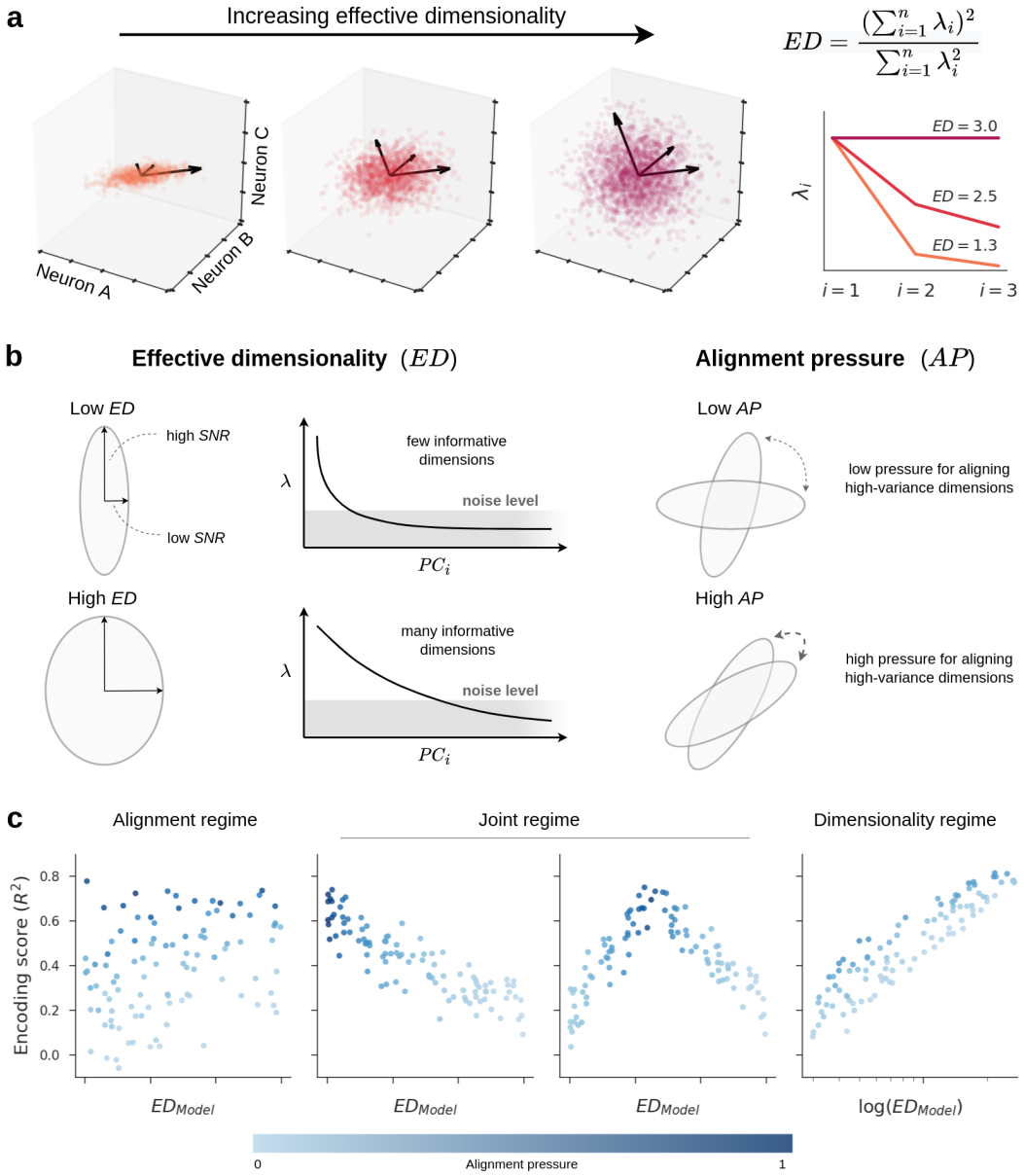

Figure 1: A theory of latent dimensionality and encoding performance. a. This panel illustrates effective dimensionality (ED) for a hypothetical population of three neurons. The data points correspond to stimuli, and the plot axes indicate the firing rates of neurons in response to these stimuli. The leftmost plot shows a scenario where the firing rates of the neurons are highly correlated and primarily extend along a single direction, resulting in an ED close to 1. The opposite scenario is shown in the rightmost plot where variance in neural responses is equally distributed across all directions, resulting in an ED of 3. On the right, we show the eigenspectra (λ_i) in each scenario and the equation that describes how ED is computed from these eigenspectra. **b.** Our simulations examine two geometric properties: effective dimensionality (ED) and alignment pressure (AP). ED is a summary statistic that indicates the number of features accurately encoded by an ecological or model subspace (i.e., it is a way of estimating latent dimensionality). The eigenspectrum of a low-dimensional subspace will decay quickly and most features will be dominated by noise and, therefore, poorly encoded, whereas the eigenspectrum of a high-dimensional subspace will have high variance spread along a large number of dimensions. AP determines the alignment of high-variance dimensions across two subspaces. Pairs of subspaces with low AP are sampled independently with little bias for their signal dimensions to align, whereas pairs of subspaces with high AP are more likely to have substantial overlapping variance along their signal dimensions. **c.** Depending on the distributions of ED and AP in empirical models, our simulations predict different outcomes for the relationship between model ED and encoding performance. *Caption continues on next page.*

Figure 1 ***(previous page)*****:** In the Alignment regime, model performance is predominantly driven by the alignment of the meaningful, signal dimensions in the model and the brain, with little to no influence of latent dimensionality. Most modeling efforts in computational neuroscience implicitly assume that models operate in the Alignment regime. Another possibility is that models operate in a Joint regime, in which there exists some optimal dimensionality at which model representations are more likely to be aligned with the brain. This is the implicit assumption behind efforts to explain brain representations with models that compress latent dimensionality (such as autoencoders). A third possibility, which has been largely overlooked, is that models operate in a Dimensionality regime, in which models with higher latent dimensionality are more likely to contain the same representational dimensions that were sampled in a neuroscience experiment. Note that the Dimensionality regime occurs when there is large variance in model ED, so we use a logarithmic scale on the x-axis for this regime.

A final possibility is that of a *Dimensionality regime*. This can occur if the computational models under consideration vary significantly in terms of ED and are sufficiently constrained to make the baseline probability of partially overlapping with visual cortex non-negligible (i.e., they have some moderate level of AP). In this case, ED will exert a strong, positive influence on expected encoding performance (Figure 1c right panel). This possibility has largely been overlooked in previous work, but it has been overlooked for good reason—the idea that a single geometric descriptor could be the key to identifying high-fidelity models of complex brain systems is surprising and is in contrast with how researchers typically describe the representational theories underlying their models, which is often in terms of architectures, learning algorithms, task objectives, and training data.

It is unknown whether ED is a governing factor for convolutional neural network models of visual cortex, and, if so, whether high-dimensional representations lead to better or worse models. Our simulations suggest several possible outcomes depending on the empirical distribution of ED and AP, including a previously unexplored scenario where high latent dimensionality is associated with better cross-validated models of neural activity. Thus, we next set out to examine this possibility using state-of-the-art DNNs and recordings of image-evoked responses in visual cortex.

2.2 Dimensionality and encoding performance for neural data

Existing hypotheses for the success of deep learning models of visual cortex include the training task, training data, architecture, and layer depth (e.g. Cadena et al., 2022; Cao & Yamins, 2021a, 2021b; Conwell et al., 2022; Dwivedi et al., 2021; Khaligh-Razavi & Kriegeskorte, 2014; Konkle & Alvarez, 2022; Kriegeskorte, 2015; Lindsay, 2020; Yamins & DiCarlo, 2016; Yamins et al., 2014; Zhuang et al., 2021). We therefore examined a large bank of 536 DNN encoding models that vary across each of these factors. The training tasks for these DNNs included a variety of objectives, spanning both supervised (e.g., object classification) and self-supervised (e.g., contrastive learning) settings. We also included untrained DNNs. The training datasets provided to these DNNs included ImageNet (Russakovsky et al., 2015) and Taskonomy (Zamir et al., 2018). All DNNs had ResNet50 or ResNet18 architectures (He, Zhang, Ren, & Sun, 2015), and we examined each convolutional layer from each network. This allowed us to examine the effect of ED while controlling for architecture. We restricted our analyses to convolutional layers because the architectures of the fully connected layers substantially differed across models. A detailed description of all models is provided in Appendix E.

We first compared these DNN models with electrophysiological recordings of image-evoked responses in macaque IT cortex—a high-level region in the ventral visual stream that supports object recognition (DiCarlo, Zoccolan, & Rust, 2012). These data were collected by Majaj, Hong, Solomon, and DiCarlo (2015), and the stimuli in this study were images of objects in various poses overlaid on natural image backgrounds. In total, the dataset consisted of 168 multiunit recordings for 3,200 stimuli. We quantified the ability of each convolutional layer in each DNN to explain neural responses by fitting unit-wise linear encoding models using partial least squares regression, which is a standard procedure in the field for mapping computational models to neural data (Yamins et al., 2014). These encoders were evaluated through cross-validation, where regression weights are learned from a training set and then used to predict neural responses to stimuli in a held-out test set (Fig. 2b). We measured encoding performance by computing the median explained variance between the predicted and actual neural responses across all recorded units.

We wanted to determine if encoding performance was related to the ED of representational subspaces in DNNs (Fig. 2). Thus, we empirically estimated the ED of the DNNs by obtaining layer activations

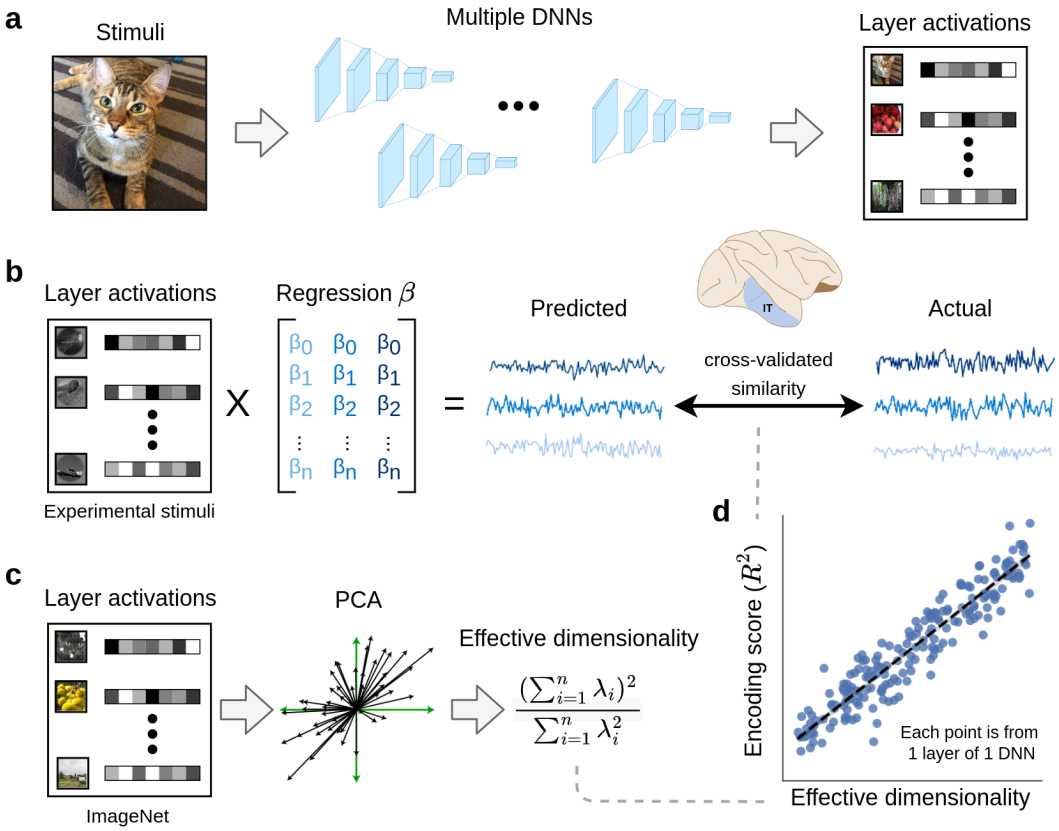

Figure 2: Method for comparing latent dimensionality with encoding performance for neural data. a. Layer activations were extracted from a large bank of DNNs trained with different tasks, datasets, and architectures. **b.** Using these layer activations as input, we fit linear encoding models to predict neural activity elicited by the same stimuli in both monkey and human visual cortex. We used cross-validation to evaluate encoding performance on unseen stimuli. **c.** To estimate the effective dimensionality of our models, we ran principal component analysis on layer activations obtained from a large dataset of naturalistic stimuli (specifically, 10,000 images from the ImageNet validation set). **d.** These analyses allowed us to examine the empirical relationship between effective dimensionality and linear encoding performance across a diverse set of DNNs and layers. DNN = deep neural network, PCA = principal component analysis.

in response to 10,000 natural images from the ImageNet validation set (Russakovsky et al., 2015). We applied PCA to these layer activations and computed ED using the eigenvalues associated with the principal components. An important methodological detail is that we applied global max-pooling to the convolutional feature maps before computing their ED. The reason for this is that we were primarily interested in the variance of image *features*, which indicates the diversity of image properties that are encoded by each model, rather than the variance in those properties across space. Nevertheless, we show in Appendix F that our main results on the relationship between ED and encoding performance were observed even when ED was computed on the entire flattened feature maps without pooling. The ED values that we computed can be interpreted as estimates of the number of meaningful dimensions of natural image representation that are encoded by each model (i.e., their latent dimensionality). Note that a central hypothesis underlying dimensionality metrics like ED is that high-variance dimensions correspond to meaningful axes in representational space while low-variance dimensions correspond to random or less-useful axes. In this framework, even deterministic systems, like the DNNs examined here, have a range of meaningfulness versus randomness across their representational axes. Indeed, previous work provides evidence that DNNs expand variance along dimensions that are useful for solving their tasks and may even contract variance along random or less-useful dimensions (Flesch, Juechems, Dumbalska, Saxe, & Summerfield, 2022; Frei, Chatterji, & Bartlett, 2022; Recanatesi et al., 2019). We provide a more detailed discussion of these points in Appendices A & J.

Our analyses of ED showed several general trends, which are discussed in detail in Appendix H. Briefly, we found that ED is higher for trained compared with untrained models, that ED tends to increase with layer depth, and that ED tends to be higher for models trained on a wide variety of natural images rather than only indoor scenes. These trends in ED suggest that feature expansion may be an important mechanism of the convolutional layers in DNNs.

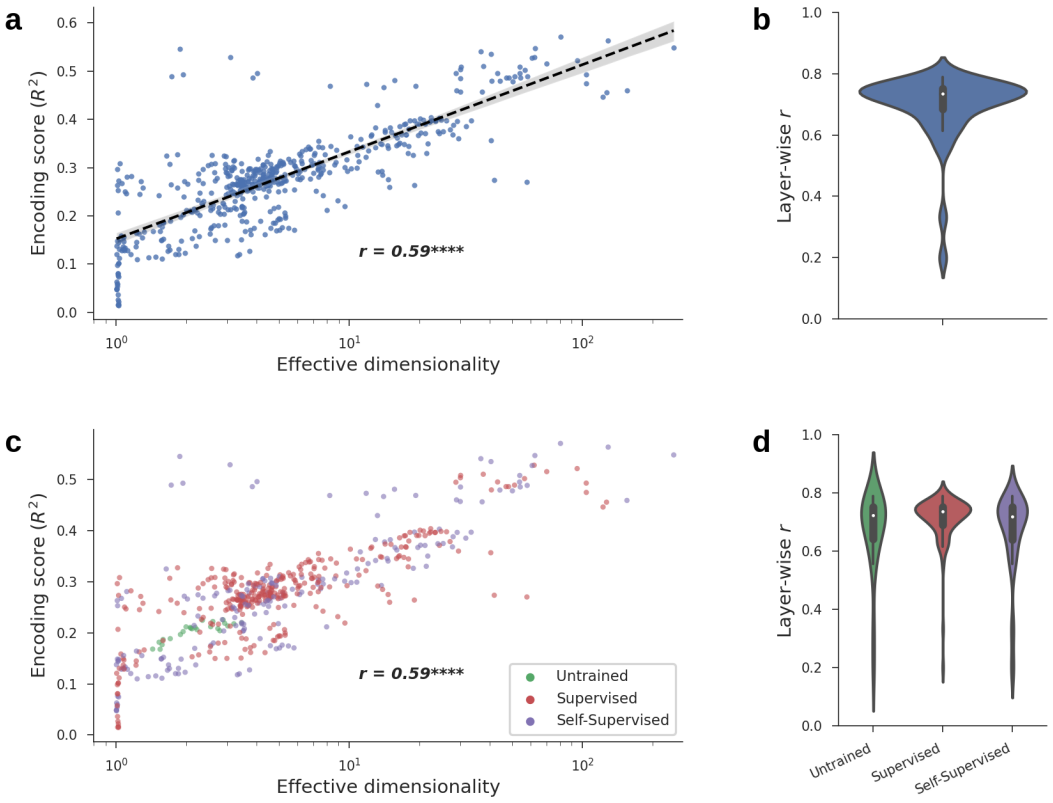

Figure 3: Relationship between effective dimensionality and encoding performance. a. The encoding performance achieved by a model scaled with its effective dimensionality (Pearson $r = 0.59$, $p < 0.0001$). Each point in the plot was obtained from one layer from one DNN, resulting in a total of 536 models. **b.** Even when conditioning on a particular DNN layer, controlling for both depth and ambient dimensionality (i.e., number of neurons), effective dimensionality and encoding performance continued to strongly correlate. The plot shows the distribution of these correlations (Pearson r) across all unique layers in our analyses. **c,d.** The above trends also held *within* different kinds of model training paradigms (supervised, self-supervised, untrained), further demonstrating the generality of the relationship between ED and encoding performance.

We next sought to determine how the ED of these DNNs compares with their encoding performance when modeling cortical responses. Our analysis revealed a clear and striking effect: the encoding performance of DNN models of visual cortex is strongly and positively correlated with ED (Fig. 3a). This effect could not be explained by differences in ED across DNN layers because it was also observed when separately examining subsets of models from the same layer (Fig. 3b). Note that this within-layer analysis also perfectly controls for ambient dimensionality, which is the number of neurons in a layer, and, thus, shows that this effect is specifically driven by the *latent* dimensionality of the representational subspaces. Furthermore, this effect could not be explained by categorical differences across learning paradigms because it was also observed when separately examining subsets of models that were either untrained, supervised, or self-supervised (Fig. 3c,d). Remarkably, this effect is not specific to the encoding model paradigm, as it was also observed when using representational similarity analysis (Kriegeskorte, Mur, & Bandettini, 2008), which involved no parameter fitting (see Appendix G). Finally, we also performed these analyses for more brain regions (V4 and V1) and for a human fMRI dataset collected by Bonner and Epstein (2021). With the exception of the monkey V1 data, we found a strong, positive relationship between ED and encoding performance across multiple datasets, thus showing a replication of this effect across

species, recording modalities, and brain regions (see Appendix F). We speculate that the effect was not observed in the monkey V1 dataset for two potential reasons. The first is that the stimuli in this V1 dataset were simple images of synthesized textures, which may not require the complexity of high ED models Freeman, Ziemba, Heeger, Simoncelli, and Movshon (2013). The second is that V1 is known to be explained by primitive edge detectors that likely emerge in most DNNs, even those with low ED. In sum, DNNs that encode a greater diversity of image features tend to yield higher-fidelity predictions of image representations in visual cortex, with the effects observed most strongly in higher-level regions.

Together, these findings show that latent dimensionality—a single geometric descriptor—can predict the likelihood that a DNN will be an accurate encoding model of visual cortex, regardless of other explanatory factors that have been emphasized in previous work, such as learning objective, training data, and layer depth.

2.3 Low-ED outliers have high latent dimensionality

In our comparison of latent dimensionality and encoding performance, we observed several notable outliers that exhibited good encoding performance despite having low ED (upper left corner in Figure 3a). To investigate this further we examined the complete eigenspectra of all models (i.e., the variance along successive principal components). Intuitively, models with more slowly decaying eigenspectra use more of their principal components to represent stimuli. In line with this, Figure 4a shows that the more slowly a model's eigenspectrum decays, the higher its encoding performance tends to be. Interestingly, the top-performing models all tend to approach a power-law eigenspectrum decaying as $\frac{1}{i}$, where i is the principal component index. This power-law decay corresponds to a proposed theoretical limit wherein features are maximally expressive and high-dimensional while still varying smoothly as a function of changing stimuli Stringer et al. (2019).

When focusing on the low-ED outliers from Figure 3, we can see that their eigenspectra are largely similar to other models with high encoding performance: beyond the first principal component, their eigenspectra decay as $\frac{1}{i}$. Why, then, do they have low ED? Figure 4b shows that, in general, models with slowly decaying eigenspectra have high ED, as expected. However, for the outliers, the disproportionately high variance along the first principal component drastically decreases their ED. Seen in this light, it is clear that the outlier models from Figure 3 are consistent with the general trend across all models: they have high latent dimensionality (i.e., slowly-decaying eigenspectra across all but their first PC) and high encoding performance. Furthermore, in Appendix I we show that the later principal components in these models are essential to their high encoding performance, which further suggests that they are in fact high-dimensional and that their low ED can be attributed to the disproportionately high-variance of their first PC.

While visual inspection of eigenspectra plots can be illuminating, it is difficult to succinctly summarize the large amount of information that these plots contain. We, therefore, we continue to use ED in our discussions below in virtue of the concise, high-level description it provides.

2.4 High dimensionality is associated with better generalization to novel categories

Our finding that top-performing encoding models of visual cortex tend to have high dimensionality was surprising given that previous work has either not considered latent dimensionality (Cadena et al., 2022; Cao & Yamins, 2021a, 2021b; Conwell et al., 2022; Dwivedi et al., 2021; Khaligh-Razavi & Kriegeskorte, 2014; Konkle & Alvarez, 2022; Kriegeskorte, 2015; Lindsay, 2020; Yamins & DiCarlo, 2016; Yamins et al., 2014; Zhuang et al., 2021) or argued for the opposite of what we discovered: namely that low-dimensional representations better account for biological vision and exhibit computational benefits in terms of robustness and categorization performance (Ansuini et al., 2019; Lehky et al., 2014). We wondered whether there might be some important computational benefits of high-dimensional subspaces that have been largely missed in the previous literature. Recent theoretical work on the geometry of high-dimensional representations suggests some hypotheses (Laakom et al., 2021; Sorscher et al., 2021; Stringer et al., 2019). Specifically, it has been proposed that increased latent dimensionality can improve the learning of novel categories, allowing a system to efficiently generalize to new categories using fewer examples (Sorscher et al., 2021). Efficient learning is critical for visual systems that need to operate in a diversity of settings with stimulus categories that cannot be fully known *a priori*, and it is something that humans and other animals

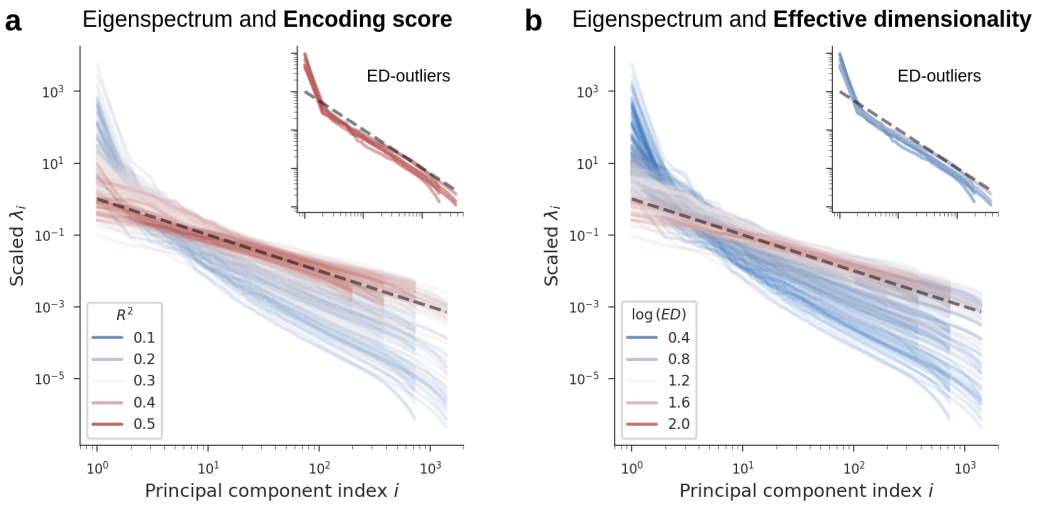

Figure 4: Relationship between model eigenspectra and encoding performance. Each curve shows the eigenspectrum of one layer from one DNN. The x-axis is the index of principal components, sorted in decreasing order of variance, and the y-axis is the variance along each principal component (scaled by a constant in order to align all curves for comparison). Inset plots show a subset of models that appear as outliers in Fig. 3 due to their high encoding performance despite low ED. The black line is a reference for a power law function that decays as $\frac{1}{i}$, where i is the principal component index. This power law of $\frac{1}{i}$ was hypothesized in Stringer et al. (2019) to be a theoretical upper limit on the latent dimensionality of smooth representations. **a.** Eigenspectra are color-coded as a function of the corresponding encoding performance each model achieved. Models with more slowly decaying eigenspectra (i.e., higher latent dimensionality) can reliably better predict neural activity, with top-performing models approaching the theoretical upper bound on dimensionality proposed in Stringer et al. (2019). **b.** Eigenspectra are color-coded as a function of their corresponding ED. Since ED is a summary statistic of an eigenspectrum meant to quantify its rate of decay, we expect models with slowly decaying eigenspectra to have higher ED. While this is generally true, some slowly decaying eigenspectra have low ED (blue curves that are near the black line). Specifically, the outliers from the upper left corner of Fig. 3a have low ED despite despite having a slow decay rate across most of the spectrum (inset). This can be explained by the disproportionately high variance along the first principal component of the outlier models, which leads to a low ED score.

are remarkably good at (Behl-Chadha, 1996; Carey & Bartlett, 1978; Quinn, Eimas, & Rosenkrantz, 1993; Smith, Jones, Landau, Gershkoff-Stowe, & Samuelson, 2002).

Thus, we examined whether the dimensionality of our DNNs was related to their generalization performance on newly learned categories. We employed a standard transfer learning paradigm in which we fixed the representations of our DNN models and tested whether they could generalize to a new target task using only a simple downstream classifier (depicted in Figure 5a). Following the approach in Sorscher et al. (2021), we trained a classifier on top of each model's representations using a simple prototype learning rule in which stimuli were predicted to belong to the nearest class centroid. We used 50 object categories from the ImageNet-21k dataset (Ridnik, Baruch, Noy, & Zelnik-Manor, 2021) and trained on 50 images per category, evaluating on another 50 held-out images from the same categories. Importantly, none of the ImageNet-21k classes appeared in any of the datasets our models were pre-trained on, allowing us to assess a relationship between the latent dimensionality of a representation and its ability to classify novel categories. The results, illustrated in Figure 5b, show a striking benefit of high-dimensionality for this task. Even though high-dimensional representations have traditionally been thought to be undesirable for object classification (Chung et al., 2018; Feng et al., 2022; I. Fischer & Alemi, 2020; I. S. Fischer, 2020; Lee et al., 2021; Recanatesi et al., 2019), they proved to be extremely effective in separating novel categories. This suggests that while low-dimensional representations may be optimal for performing specialized tasks (such as separating the fixed set of categories in the standard ImageNet training set), high-dimensional representations may be more flexible and better suited to support open-ended tasks (Brown et al., 2020; Flesch et al., 2022; Fusi et al., 2016; Higgins, Racanière, & Rezende, 2022; Sorscher et al., 2021).

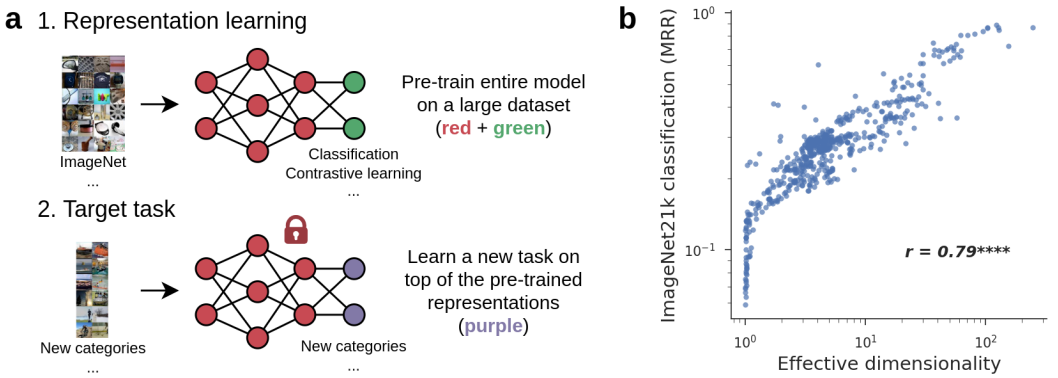

Figure 5: The computational benefit of high effective dimensionality in generalization to new object categories. We examined the hypothesis that high-dimensional representations are better at learning to classify new object categories (Sorscher et al., 2021). **a.** We tested this theory using a transfer learning paradigm, where our pre-trained model representations were fixed and used to classify novel categories through a prototype learning rule. **b.** Our high-dimensional models achieved substantially better accuracy on this transfer task, as measured using the mean reciprocal rank (MRR).

3 High dimensionality concentrates projection distances along linear readout dimensions

How do high-dimensional models achieve better classification performance for novel categories? If we consider an idealized scenario in which categories are represented by spherical or elliptical subspaces, it is a geometric fact that projections of these subspaces onto linear readout dimensions will concentrate more around their subspace centroids as dimensionality increases (assuming that the radius is held constant) (Gorban, Makarov, & Tyukin, 2020; Gorban & Tyukin, 2018; Sorscher et al., 2021). The reason for this is that in high dimensions, most of the subspace's mass is concentrated along its equator, orthogonal to the linear readout dimension. This blessing of dimensionality is typically referred to as the *concentration of measure phenomenon* (Gorban & Tyukin, 2018), and we depict it for the case of idealized spherical subspace in Figure 6a,b.

Although we do not know the geometric shapes of category subspaces in DNNs or whether they can be approximated by elliptical subspaces, we can, nonetheless, test whether there is empirical evidence that a similar concentration phenomenon occurs in our models. To answer this question, we computed the average sample projection distance between every pair of our 50 ImageNet-21k classes, normalized by an estimate of the subspace radius for each class (see Section 5, Materials and Methods). This yielded a matrix of all pairwise projection distances for each model. Figure 6c shows that, as predicted, the mean projection distance systematically decreases as model ED increases. This means that sample projection distances concentrate closer to class centroids as model dimensionality increases, allowing DNNs with higher ED to discriminate novel categories more effectively. This concentration effect exemplifies an underappreciated computational advantage conferred by the geometric properties of high-dimensional subspaces.

4 Discussion

By computing geometric descriptors of DNNs and performing large-scale model comparisons, we discovered a geometric phenomenon that has been overlooked in previous work: DNN models of visual cortex benefit from high-dimensional latent representations. This finding runs counter to the view that both DNNs and neural systems benefit by compressing representations down to low-dimensional subspaces (Amsaleg et al., 2017; Ansuini et al., 2019; Churchland et al., 2012; Feng et al., 2022; I. Fischer & Alemi, 2020; I. S. Fischer, 2020; Gallego et al., 2017; Gao & Ganguli, 2015; Gao et al., 2017; Gong et al., 2019; Kingma & Welling, 2013; Lee et al., 2021; Lehky et al., 2014; Ma et al., 2018; Nieh et al., 2021; Op de Beeck et al., 2001; Pope et al., 2021; Recanatesi et al., 2019; Saxena & Cunningham, 2019; Tishby & Zaslavsky, 2015; Zhu et al., 2018). Furthermore, our findings suggest that the design factors that have been a major focus of previous work, such as

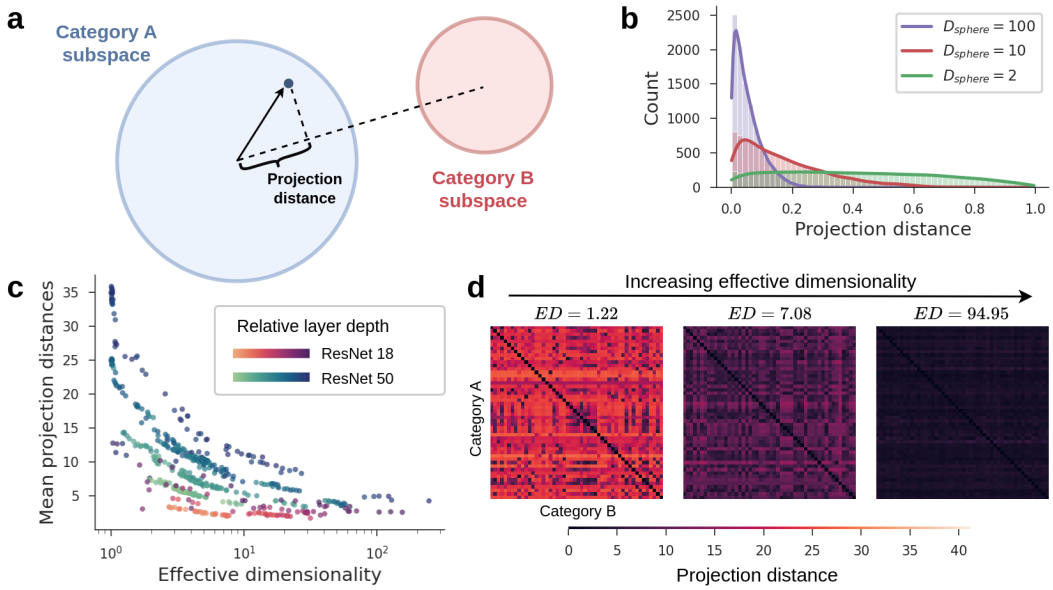

Figure 6: High-dimensional models concentrate sample projections close to their class centroids. a. For binary classification of samples distributed within class subspaces, the projection distance of a sample refers to its distance to the true class centroid along the classification readout direction, normalized by the subspace radius. **b.** For idealized spherical subspace, the distribution of projection distances concentrates more tightly around 0 as the dimensionality D_{sphere} increases. **c.** Empirically, the mean projection distances of our models decreased as effective dimensionality increased, matching what is predicted by theory. Note that because the magnitude of projections partially depend on the model architecture and layer depth (denoted by different colors), projection distances form distinct bands in the plot. However, when looking only at models with the same architecture and layer (i.e., looking at points sharing the same color), projection distances reliably decrease with ED. **d.** Full projection distance matrices, computed along classification readout directions between all object category pairs. Matrices are shown for three different models of increasing effective dimensionality.

architecture and training, are of secondary importance and are best understood in the context of how they influence representational dimensionality. Thus, geometric descriptors offer a powerful level of explanation that can predict the encoding performance of DNN models of visual cortex and abstract over the details of their architectures, training data, and learning objectives.

Our results speak to a fundamental question about the dimensionality of neural population codes. Empirical estimates have consistently shown that the latent dimensionality of both DNNs and neural systems is orders of magnitude lower than their ambient dimensionality (i.e., the number of neurons they contain) (Ansuini et al., 2019; Churchland et al., 2012; Cohen et al., 2020; Feng et al., 2022; Gallego et al., 2018; Gao & Ganguli, 2015; Gao et al., 2017; Gong et al., 2019; Lehky et al., 2014; Nieh et al., 2021; Op de Beeck et al., 2001). Furthermore, there are compelling theoretical arguments for the computational benefits of low-dimensional codes, which may promote robustness to noise (Amsaleg et al., 2017; I. Fischer & Alemi, 2020; Lee et al., 2021; Ma et al., 2018; Recanatesi et al., 2019; Zhu et al., 2018), abstraction and invariance (I. S. Fischer, 2020; Gallego et al., 2017, 2018; Kingma & Welling, 2013; Tishby & Zaslavsky, 2015), compactness (Cohen et al., 2020), and learnability for downstream readouts (Abu-Mostafa, 2012, i.e., avoiding the curse of dimensionality). It is, thus, no surprise that many neuroscientists and machine learning researchers have argued that a signature of optimal population codes is the degree to which they reduce latent dimensionality, focusing on the minimum components needed to carry out their functions. However, there are competing theoretical arguments for the benefits of high-dimensional population codes. High-dimensional codes are more efficient (Barlow, 1961; Olshausen & Field, 1996), they allow for the expression of a wider variety of downstream readouts (Fusi et al., 2016), and they may have counter-intuitive benefits for learning new categories due to concentration phenomena in high dimensions (Sorscher et al., 2021). Furthermore, recent evidence from large-scale data in mouse visual cortex suggests that cortical population codes are higher dimensional than previously reported and may, in fact, approach a theoretical limit, above which the code would no longer be smooth (Stringer et

al., 2019). Our findings provide strong evidence for the benefits of high-dimensional population codes. Specifically, we demonstrate two major benefits that are directly relevant to computational neuroscientists. First, high-dimensional DNNs provide more accurate cross-validated predictions of cortical image representations. In fact, when looking at the eigenspectra of our top-performing models, they appear to approach the upper limit on dimensionality that was proposed in Stringer et al. (2019). Second, high-dimensional DNNs are more effective at learning to classify new object categories. We suggest that while low-dimensional codes may be optimal for solving specific, constrained tasks on a limited set of categories, high-dimensional codes may function as general-purpose representations, allowing them to better support an open-ended set of downstream tasks and stimuli.

Our findings also have implications for how neuroscientists interpret the relationship between DNNs and neural representations. When developing theories to explain why some DNNs are better than others as computational brain models, it is common for researchers to place a strong emphasis on the role of design factors, such as architecture, training data, and learning objective (Cadena et al., 2022; Cao & Yamins, 2021a, 2021b; Conwell et al., 2022; Dwivedi et al., 2021; Khaligh-Razavi & Kriegeskorte, 2014; Konkle & Alvarez, 2022; Kriegeskorte, 2015; Lindsay, 2020; Yamins & DiCarlo, 2016; Yamins et al., 2014; Zhuang et al., 2021). However, our findings suggest that these design factors may be of secondary importance, with geometric factors best explaining the relationship between DNNs and neural representations. Indeed, we found that a variety of design configurations, spanning different architectures, layers, training data, and learning objectives, are sufficient to yield high-performing encoding models of visual cortex. However, when analyzing the geometry of these networks, we found that a common thread running through the best-performing models was their strong tendency to encode high-dimensional subspaces. It is worth emphasizing that we were only able to observe this phenomenon by analyzing the geometry of latent representations and by performing large-scale comparisons across diverse DNNs. In other words, the most important factors for explaining model performance were not evident in the surface properties of an single model but rather in their latent statistics. This findings is consistent with other recent work showing that widely varying learning objectives and architectures—including transformer architectures from computational linguistics—are sufficient to produce state-of-the-art encoding performance in visual cortex, which suggests that these design factors are not the primary explanation for the success of DNNs in visual neuroscience (Conwell et al., 2022; Konkle & Alvarez, 2022; Zhuang et al., 2021). Our findings are also consistent with recent work that calls into question the apparent hierarchical correspondence between DNNs and visual cortex (Sexton & Love, 2021). Indeed, we found that the relationship between latent dimensionality and encoding performance generalized across layer depth, meaning that even within a single layer of a DNN hierarchy, encoding performance can widely vary as a function of latent dimensionality. Thus, our work suggests that the geometry of latent representations offers a promising approach for discovering unified explanations of diverse computational brain models and for abstracting over the details of their architectures and training. Importantly, we predict that accurate computational models of the brain may necessarily need to have high-dimensional latent representations.

Our results raise several important questions for future work. First, while our findings show that computational models of visual cortex benefit from high latent dimensionality, they cannot speak to the dimensionality of visual cortex itself. However, our findings suggest a promising model-guided approach for tackling this issue: one could use high-dimensional DNNs to create stimulus sets that vary along as many orthogonal dimensions as possible. This sets up a critical test of whether the latent dimensionality of visual cortex scales up to the dimensionality of the model or, instead, hits a lower-dimensional ceiling. Second, we found that one way in which DNNs can achieve both strong encoding performance and strong image classification performance is by increasing the latent dimensionality of their representations, but this finding diverges from previous work that has linked better classification performance to dimensionality reduction in DNN representations (Ansuini et al., 2019; Recanatesi et al., 2019). We believe that this discrepancy arises due to a fundamental problem with classification metrics: DNNs with the best classification scores are optimal for a single task on a small and closed set of categories (e.g., ImageNet classes), but these seemingly optimal DNNs may be far less useful for representing new categories or for representing meaningful variance within a category (e.g., object pose). This problem with classification metrics may help to explain why the strong correlation between DNN classification performance and cortical encoding performance (Yamins et al., 2014; Zhuang et al., 2021) appears to break down at the highest levels of classification accuracy (Schrimpf et al., 2018, 2020) (see an extended discussion of these issues in Appendix A). Finally, an important open question is whether our results are specific to convolutional

neural networks and visual cortex or whether similar results could be obtained for other classes of computational models (e.g., Transformers, generative models) and other sensory and cognitive domains (e.g., audition, language).

The computational problems of real-world vision may demand high-dimensional representations that sacrifice the competing benefits of robust, low-dimensional codes. Indeed, our findings reveal striking benefits for high dimensionality: both cortical encoding performance and novel category learning scale with the latent dimensionality of a network's natural image representations. We predict that these benefits extend further and that high-dimensional representations may be essential for handling the open-ended set of tasks that emerge over the course of an agent's lifetime (Brown et al., 2020; Flesch et al., 2022; Fusi et al., 2016; Higgins et al., 2022; Sorscher et al., 2021).

5 Materials and Methods

Simulations The theory and rationale behind our simulations is explained in Appendix B. Precise implementation details are provided in Appendix C.

Deep neural networks We used 40 different pre-trained DNNs, each with either a ResNet18 or a ResNet50 architecture. Training tasks included supervised (e.g., object classification) and self-supervised (e.g., colorization) settings. We also used untrained models with randomly initialized weights. The training datasets of these DNNs included ImageNet (Russakovsky et al., 2015) and Taskonomy (Zamir et al., 2018). Further details describing each model are provided in Appendix E. Convolutional layers in ResNets are arranged into 4 successive groups, each with a certain number of repeated computational units called blocks. We extracted activations from the outputs of each of these computational blocks, of which there are 8 in ResNet18 and 16 in ResNet50. Across our 40 DNNs, this resulted in a total of 536 convolutional layers that we used for all further analyses.

Neural datasets Neural responses were obtained from a publicly available dataset collected by Majaj et al. (2015). Two fixating macaques were implanted with two arrays of electrodes in IT—a visual cortical region in later stages of the ventral-temporal stream—resulting in a total of 168 multiunit recordings. Stimuli consisted of artificially-generated gray-scale images composed from 64 cropped objects belonging to 8 categories, which were pasted atop natural scenes at various locations, orientations, and scales. In total, the dataset held responses to 3,200 unique stimuli.

In Appendix F, we also show results on additional datasets. The V4 electrophysiology dataset was collected in the same study as for IT (Majaj et al., 2015). The V1 electrophysiology dataset was collected by Freeman et al. (2013), and consisted of responses to 9000 simple synthetic texture stimuli. In addition to our electrophysiology datasets, we also used a human fMRI dataset collected by Bonner and Epstein (2021). The stimulus set consisted of 810 objects from 81 different categories (10 object tokens per category). fMRI responses were measured while 4 subjects viewed these objects, shown alone on meaningless textured backgrounds, and performed a simple perceptual task of responding by button press whenever they saw a "warped" object. Warped objects were created through diffeomorphic warping of object stimuli (Stojanoski & Cusack, 2014). The methods for identifying regions of interest in these data are detailed in Bonner and Epstein (2021). The localizer scans for these data did not contain body images, and, thus, a contrast of faces-vs.-objects was used to select voxels from the parcel for the extrastriate body area (EBA).

Predicting neural responses We obtained activations at a particular layer of a DNN to the same stimuli that were used for obtaining neural responses. The output for each stimulus was a three-dimensional feature map of activations with shape $channels \times height \times width$, which we flattened into a vector. For our monkey electrophysiology dataset, we fit a linear encoding model to predict actual neural responses from the DNN layer features through partial-least-squares regression with 25 latent components, as in Yamins et al. (2014) and Schrimpf et al. (2018). To measure the performance of these encoding models, we computed the Pearson correlation between the predicted and actual neural responses on held-out data using 10-fold cross validation, and averaged these correlations across folds. We aggregated the per-neuron correlations into a single value by taking the median, which we then normalized by the median noise ceiling (split-half reliability) across all neurons. This normalization was done by taking the squared quotient $r^2 = (r/r_{ceil})^2$, converting our final encoding score into a coefficient of explained variance relative to the noise ceiling. The entire process described

above for fitting linear encoding models was implemented with the Brain-Score package (Schrimpf et al., 2018, 2020) using default arguments for the Majaj et al. (2015) public benchmark.

The process for fitting voxel-wise encoding models of human fMRI data (presented in Appendix F) differed slightly from above. For each of our 4 subjects, we used 9-fold cross-validated ordinary least squares regression. Encoding performance was measured by taking the mean Pearson correlation between predicted and held-out voxel responses across folds, and then aggregated by taking the median across voxels. Finally, this score was averaged across subjects. No noise-ceiling normalization was used.

Before fitting these linear encoding models, we also applied PCA to the input features in order to keep the number of parameters in the encoders constant. For each model layer, principal components were estimated using 1000 images from the ImageNet validation set. Layer activations to stimuli from the neural dataset were then projected along 1000 components and finally used as regressors when fitting linear encoding models. We emphasize that this dimensionality reduction procedure was done purely for computational reasons, as using fewer regressors reduced the computer memory and time required to fit our encoding models. Our findings are not sensitive to this particular decision, as we obtained similar results by applying max-pooling instead of PCA to our DNN feature maps as an alternative method for reducing the number of regressors.

Estimating latent dimensionality We used a simple linear metric called effective dimensionality (ED) (Giudice, 2021) to estimate the latent dimensionality of our model representations. ED is given by a formula that quantifies roughly how many principal components contribute to the total variance of a representation. We, thus, ran PCA on the activations of a given model layer in response to a large number of natural images (10,000 from the ImageNet validation set) in an effort to accurately estimate its principal components and the variance they explain. An important methodological detail is that we applied global max-pooling to the convolutional feature maps before computing their ED. The reason for this is that we were primarily interested in the variance of image *features*, which indicates the diversity of image properties that are encoded by each model, rather than the variance in those properties across space.

Classifying novel object categories To see how model ED affected generalization to the task of classifying novel object categories, we used a transfer learning paradigm following Sorscher et al. (2021). For a given model layer, we obtained activations to images from $M = 50$ different categories each with $N_{train} = 50$ samples. We then computed M category prototypes by taking the average activation pattern within each category. These prototypes were used to classify $N_test = 50$ novel stimuli from each category according to a simple rule, in which stimuli were predicted to belong to the nearest prototype as measured by Euclidean distance. This process was repeated for 10 iterations of Monte Carlo cross-validation, after which we computed the average test accuracy. Importantly, none of these object categories or their stimuli appeared in any of the models' pre-training datasets. Stimuli were taken from the ImageNet-21k dataset (Ridnik et al., 2021), and our object categories were a subset of those used in Sorscher et al. (2021).

Projection distances along readout dimensions Appendix 3 investigated how points sampled from high-dimensional object subspaces project along linear readout vectors. We sampled 50 random images from the same 50 ImageNet-21k object categories described above. For every pair of object categories i and j, we created a classification readout vector $\mathbf{w}_{i,j}$ by taking the difference between category centroids normalized to unit length. This is the readout vector along which samples would be projected using a prototype learning classification rule. We then projected each sample k in category i along the readout vector, yielding a scalar projection distance to the category centroid $p^k_{i,j}$. We took the mean of all 50 sample projections and normalized them by the mean standard deviation along all category subspace dimensions in order to see how closely samples projected to their category centroids relative to the subspace radius. We refer to the resulting values as the mean normalized projection distances $\bar{p}_{ij}$. For $i, j = 1, .., 50$ object categories, this procedure yields a 50×50 matrix $\bar{P}$ for each model. Figure 6d shows examples of these matrices for models of increasing ED. The means of these matrices as a function of ED are shown for all models in Figure 6c.

Data availability The neural electrophysiology datasets are publicly available and was collected in prior work by Majaj et al. (2015) and Freeman et al. (2013). It is imported automatically using the BrainScore version 0.2 Python library through code in our publicly available project repository. The

fMRI data was collected in prior work by Bonner and Epstein (2021) and is publicly available here: `https://osf.io/ug5zd/`.

Code availability All code used for this project has been made publicly available on GitHub `https://github.com/EricElmoznino/encoder_dimensionality`.

Acknowledgments and Disclosure of Funding

The brain icon in Fig. 2 was obtained from Smith Breault (2020).

References

Abu-Mostafa, Y. (2012, April). *Lecture notes from machine learning course: Learning from data (lecture 7).* Caltech. Retrieved from `https://home.work.caltech.edu/lectures.html`

Amsaleg, L., Bailey, J., Barbe, D., Erfani, S., Houle, M. E., Nguyen, V., & Radovanović, M. (2017). The vulnerability of learning to adversarial perturbation increases with intrinsic dimensionality. In *2017 ieee workshop on information forensics and security (wifs)* (p. 1-6). doi: 10.1109/WIFS.2017.8267651

Ansuini, A., Laio, A., Macke, J. H., & Zoccolan, D. (2019). Intrinsic dimension of data representations in deep neural networks. *CoRR*, *abs/1905.12784*. Retrieved from `http://arxiv.org/abs/1905.12784`

Barlow, H. B. (1961). Possible principles underlying the transformations of sensory messages. In (chap. 13). The MIT Press. Retrieved from `https://doi.org/10.7551/mitpress/9780262518420.003.0013` doi: 10.7551/mitpress/9780262518420.003.0013

Barwich, A.-S. (2019, Oct 24). The value of failure in science: The story of grandmother cells in neuroscience. *Frontiers in neuroscience*, *13*, 1121-1121. Retrieved from `https://doi.org/10.3389/fnins.2019.01121` (31708726[pmid]) doi: 10.3389/fnins.2019.01121

Behl-Chadha, G. (1996, August). Basic-level and superordinate-like categorical representations in early infancy. *Cognition*, *60*(2), 105–141.

Bonner, M. F., & Epstein, R. A. (2021, Jul 02). Object representations in the human brain reflect the co-occurrence statistics of vision and language. *Nature Communications*, *12*(1), 4081. Retrieved from `https://doi.org/10.1038/s41467-021-24368-2` doi: 10.1038/s41467-021-24368-2

Brown, T. B., Mann, B., Ryder, N., Subbiah, M., Kaplan, J., Dhariwal, P., ... Amodei, D. (2020). Language models are few-shot learners. *CoRR*, *abs/2005.14165*. Retrieved from `https://arxiv.org/abs/2005.14165`

Cadena, S. A., Willeke, K. F., Restivo, K., Denfield, G., Sinz, F. H., Bethge, M., ... Ecker, A. S. (2022, May). *Diverse task-driven modeling of macaque V4 reveals functional specialization towards semantic tasks* (preprint). Neuroscience. Retrieved 2022-06-24, from `http://biorxiv.org/lookup/doi/10.1101/2022.05.18.492503` doi: 10.1101/2022.05.18.492503

Cao, R., & Yamins, D. (2021a). *Explanatory models in neuroscience: Part 1 – taking mechanistic abstraction seriously.* arXiv. Retrieved from `https://arxiv.org/abs/2104.01490` doi: 10.48550/ARXIV.2104.01490

Cao, R., & Yamins, D. (2021b). *Explanatory models in neuroscience: Part 2 – constraint-based intelligibility.* arXiv. Retrieved from `https://arxiv.org/abs/2104.01489` doi: 10.48550/ARXIV.2104.01489

Carey, S., & Bartlett, E. J. (1978). Acquiring a single new word..

Chung, S., & Abbott, L. F. (2021, October). Neural population geometry: An approach for understanding biological and artificial neural networks. *Current Opinion in Neurobiology*, *70*, 137–144. Retrieved 2022-05-22, from `http://arxiv.org/abs/2104.07059` (arXiv:2104.07059 [cs, q-bio]) doi: 10.1016/j.conb.2021.10.010

Chung, S., Lee, D. D., & Sompolinsky, H. (2018, Jul). Classification and geometry of general perceptual manifolds. *Phys. Rev. X*, *8*, 031003. Retrieved from `https://link.aps.org/doi/10.1103/PhysRevX.8.031003` doi: 10.1103/PhysRevX.8.031003

Churchland, M. M., Cunningham, J. P., Kaufman, M. T., Foster, J. D., Nuyujukian, P., Ryu, S. I., & Shenoy, K. V. (2012, Jul 01). Neural population dynamics during reaching. *Nature*, *487*(7405), 51-56. Retrieved from `https://doi.org/10.1038/nature11129` doi: 10.1038/nature11129

Cohen, U., Chung, S., Lee, D. D., & Sompolinsky, H. (2020, Feb 06). Separability and geometry of object manifolds in deep neural networks. *Nature Communications*, *11*(1), 746. Retrieved from https://doi.org/10.1038/s41467-020-14578-5 doi: 10.1038/s41467-020-14578-5

Conwell, C., Prince, J. S., Alvarez, G. A., & Konkle, T. (2022). Large-scale benchmarking of diverse artificial vision models in prediction of 7t human neuroimaging data. *bioRxiv*. Retrieved from https://www.biorxiv.org/content/early/2022/03/29/2022.03.28.485868 doi: 10.1101/2022.03.28.485868

DiCarlo, J., Zoccolan, D., & Rust, N. (2012). How does the brain solve visual object recognition? *Neuron*, *73*(3), 415-434. Retrieved from https://www.sciencedirect.com/science/article/pii/S089662731200092X doi: https://doi.org/10.1016/j.neuron.2012.01.010

Dwivedi, K., Bonner, M. F., Cichy, R. M., & Roig, G. (2021, 08). Unveiling functions of the visual cortex using task-specific deep neural networks. *PLOS Computational Biology*, *17*(8), 1-22. Retrieved from https://doi.org/10.1371/journal.pcbi.1009267 doi: 10.1371/journal.pcbi.1009267

Feng, R., Zheng, K., Huang, Y., Zhao, D., Jordan, M., & Zha, Z.-J. (2022). *Rank diminishing in deep neural networks.* arXiv. Retrieved from https://arxiv.org/abs/2206.06072 doi: 10.48550/ARXIV.2206.06072

Fischer, I., & Alemi, A. A. (2020). CEB improves model robustness. *CoRR*, *abs/2002.05380*. Retrieved from https://arxiv.org/abs/2002.05380

Fischer, I. S. (2020). The conditional entropy bottleneck. *CoRR*, *abs/2002.05379*. Retrieved from https://arxiv.org/abs/2002.05379

Flesch, T., Juechems, K., Dumbalska, T., Saxe, A., & Summerfield, C. (2022). Orthogonal representations for robust context-dependent task performance in brains and neural networks. *Neuron*, *110*(7), 1258-1270.e11. Retrieved from https://www.sciencedirect.com/science/article/pii/S0896627322000058 doi: https://doi.org/10.1016/j.neuron.2022.01.005

Freeman, J., Ziemba, C. M., Heeger, D. J., Simoncelli, E. P., & Movshon, J. A. (2013). A functional and perceptual signature of the second visual area in primates. *Nature neuroscience*, *16*(7), 974–981.

Frei, S., Chatterji, N. S., & Bartlett, P. L. (2022). *Random feature amplification: Feature learning and generalization in neural networks.* arXiv. Retrieved from https://arxiv.org/abs/2202.07626 doi: 10.48550/ARXIV.2202.07626

Fusi, S., Miller, E. K., & Rigotti, M. (2016). Why neurons mix: high dimensionality for higher cognition. *Current Opinion in Neurobiology*, *37*, 66-74. Retrieved from https://www.sciencedirect.com/science/article/pii/S0959438816000118 (Neurobiology of cognitive behavior) doi: https://doi.org/10.1016/j.conb.2016.01.010

Gallego, J. A., Perich, M. G., Miller, L. E., & Solla, S. A. (2017, June). Neural Manifolds for the Control of Movement. *Neuron*, *94*(5), 978–984. Retrieved 2022-06-14, from https://linkinghub.elsevier.com/retrieve/pii/S0896627317304634 doi: 10.1016/j.neuron.2017.05.025

Gallego, J. A., Perich, M. G., Naufel, S. N., Ethier, C., Solla, S. A., & Miller, L. E. (2018, Oct 12). Cortical population activity within a preserved neural manifold underlies multiple motor behaviors. *Nature Communications*, *9*(1), 4233. Retrieved from https://doi.org/10.1038/s41467-018-06560-z doi: 10.1038/s41467-018-06560-z

Gao, P., & Ganguli, S. (2015, April). On simplicity and complexity in the brave new world of large-scale neuroscience. *Curr Opin Neurobiol*, *32*, 148–155.

Gao, P., Trautmann, E., Yu, B., Santhanam, G., Ryu, S., Shenoy, K., & Ganguli, S. (2017). A theory of multineuronal dimensionality, dynamics and measurement. *bioRxiv*. Retrieved from https://www.biorxiv.org/content/early/2017/11/12/214262 doi: 10.1101/214262

Giudice, M. D. (2021). Effective dimensionality: A tutorial. *Multivariate Behavioral Research*, *56*(3), 527-542. Retrieved from https://doi.org/10.1080/00273171.2020.1743631 (PMID: 32223436) doi: 10.1080/00273171.2020.1743631

Gong, S., Boddeti, V. N., & Jain, A. K. (2019, June). On the Intrinsic Dimensionality of Image Representations. In *2019 IEEE/CVF Conference on Computer Vision and Pattern Recognition (CVPR)* (pp. 3982–3991). Long Beach, CA, USA: IEEE. Retrieved 2022-06-15, from https://ieeexplore.ieee.org/document/8953348/ doi: 10.1109/CVPR.2019.00411

Gorban, A. N., Makarov, V. A., & Tyukin, I. Y. (2020, January). High-Dimensional brain in a High-Dimensional world: Blessing of dimensionality. *Entropy (Basel)*, *22*(1).

Gorban, A. N., & Tyukin, I. Y. (2018). Blessing of dimensionality: mathematical foundations of the statistical physics of data. *Philosophical Transactions of the Royal Society*

A: Mathematical, Physical and Engineering Sciences, *376*(2118), 20170237. Retrieved from https://royalsocietypublishing.org/doi/abs/10.1098/rsta.2017.0237 doi: 10.1098/rsta.2017.0237

Hassabis, D., Kumaran, D., Summerfield, C., & Botvinick, M. (2017). Neuroscience-inspired artificial intelligence. *Neuron*, *95*(2), 245-258. Retrieved from https://www.sciencedirect.com/science/article/pii/S0896627317305093 doi: https://doi.org/10.1016/j.neuron.2017.06.011

He, K., Zhang, X., Ren, S., & Sun, J. (2015). Deep residual learning for image recognition. *CoRR*, *abs/1512.03385*. Retrieved from http://arxiv.org/abs/1512.03385

Higgins, I., Racanière, S., & Rezende, D. (2022). *Symmetry-based representations for artificial and biological general intelligence.* arXiv. Retrieved from https://arxiv.org/abs/2203.09250 doi: 10.48550/ARXIV.2203.09250

Jazayeri, M., & Ostojic, S. (2021). Interpreting neural computations by examining intrinsic and embedding dimensionality of neural activity. *Current Opinion in Neurobiology*, *70*, 113-120. Retrieved from https://www.sciencedirect.com/science/article/pii/S0959438821000933 doi: https://doi.org/10.1016/j.conb.2021.08.002

Khaligh-Razavi, S.-M., & Kriegeskorte, N. (2014, 11). Deep supervised, but not unsupervised, models may explain it cortical representation. *PLOS Computational Biology*, *10*(11), 1-29. Retrieved from https://doi.org/10.1371/journal.pcbi.1003915 doi: 10.1371/journal.pcbi.1003915

Kingma, D. P., & Welling, M. (2013). *Auto-encoding variational bayes.* arXiv. Retrieved from https://arxiv.org/abs/1312.6114 doi: 10.48550/ARXIV.1312.6114

Konkle, T., & Alvarez, G. A. (2022, Jan 25). A self-supervised domain-general learning framework for human ventral stream representation. *Nature Communications*, *13*(1), 491. Retrieved from https://doi.org/10.1038/s41467-022-28091-4 doi: 10.1038/s41467-022-28091-4

Kriegeskorte, N. (2015, Nov). Deep Neural Networks: A New Framework for Modeling Biological Vision and Brain Information Processing. *Annu Rev Vis Sci*, *1*, 417–446.

Kriegeskorte, N., Mur, M., & Bandettini, P. (2008). Representational similarity analysis - connecting the branches of systems neuroscience. *Frontiers in Systems Neuroscience*, *2*. Retrieved from https://www.frontiersin.org/article/10.3389/neuro.06.004.2008 doi: 10.3389/neuro.06.004.2008

Laakom, F., Raitoharju, J., Iosifidis, A., & Gabbouj, M. (2021). Within-layer diversity reduces generalization gap. *CoRR*, *abs/2106.06012*. Retrieved from https://arxiv.org/abs/2106.06012

Lee, K., Arnab, A., Guadarrama, S., Canny, J. F., & Fischer, I. (2021). Compressive visual representations. *CoRR*, *abs/2109.12909*. Retrieved from https://arxiv.org/abs/2109.12909

Lehky, S. R., Kiani, R., Esteky, H., & Tanaka, K. (2014, 10). Dimensionality of Object Representations in Monkey Inferotemporal Cortex. *Neural Computation*, *26*(10), 2135-2162. Retrieved from https://doi.org/10.1162/NECO_a_00648 doi: 10.1162/NECO_a_00648

Lindsay, G. (2020, February). Convolutional Neural Networks as a Model of the Visual System: Past, Present, and Future. *Journal of Cognitive Neuroscience*, 1–15. Retrieved 2020-02-11, from https://www.mitpressjournals.org/doi/abs/10.1162/jocn_a_01544 doi: 10.1162/jocn_a_01544

Ma, X., Li, B., Wang, Y., Erfani, S. M., Wijewickrema, S., Schoenebeck, G., ... Bailey, J. (2018). *Characterizing adversarial subspaces using local intrinsic dimensionality.* arXiv. Retrieved from https://arxiv.org/abs/1801.02613 doi: 10.48550/ARXIV.1801.02613

Majaj, N. J., Hong, H., Solomon, E. A., & DiCarlo, J. J. (2015). Simple learned weighted sums of inferior temporal neuronal firing rates accurately predict human core object recognition performance. *Journal of Neuroscience*, *35*(39), 13402–13418. Retrieved from https://www.jneurosci.org/content/35/39/13402 doi: 10.1523/JNEUROSCI.5181-14.2015

Nieh, E. H., Schottdorf, M., Freeman, N. W., Low, R. J., Lewallen, S., Koay, S. A., ... Tank, D. W. (2021, Jul 01). Geometry of abstract learned knowledge in the hippocampus. *Nature*, *595*(7865), 80-84. Retrieved from https://doi.org/10.1038/s41586-021-03652-7 doi: 10.1038/s41586-021-03652-7

Olshausen, B. A., & Field, D. J. (1996, Jun 01). Emergence of simple-cell receptive field properties by learning a sparse code for natural images. *Nature*, *381*(6583), 607-609. Retrieved from https://doi.org/10.1038/381607a0 doi: 10.1038/381607a0

Op de Beeck, H., Wagemans, J., & Vogels, R. (2001, Dec 01). Inferotemporal neurons represent low-

dimensional configurations of parameterized shapes. *Nature Neuroscience*, *4*(12), 1244-1252. Retrieved from https://doi.org/10.1038/nn767 doi: 10.1038/nn767

Paszke, A., Gross, S., Massa, F., Lerer, A., Bradbury, J., Chanan, G., ... Chintala, S. (2019). Pytorch: An imperative style, high-performance deep learning library. In H. Wallach, H. Larochelle, A. Beygelzimer, F. d'Alché-Buc, E. Fox, & R. Garnett (Eds.), *Advances in neural information processing systems 32* (pp. 8024–8035). Curran Associates, Inc. Retrieved from http://papers.neurips.cc/paper/9015-pytorch-an-imperative-style-high-performance-deep-learning-library.pdf

Pope, P., Zhu, C., Abdelkader, A., Goldblum, M., & Goldstein, T. (2021, April). The Intrinsic Dimension of Images and Its Impact on Learning. *arXiv:2104.08894 [cs, stat]*. Retrieved 2022-05-31, from http://arxiv.org/abs/2104.08894 (arXiv: 2104.08894)

Quinn, P. C., Eimas, P. D., & Rosenkrantz, S. L. (1993). Evidence for representations of perceptually similar natural categories by 3-month-old and 4-month-old infants. *Perception*, *22*(4), 463–475.

Recanatesi, S., Farrell, M., Advani, M., Moore, T., Lajoie, G., & Shea-Brown, E. (2019). Dimensionality compression and expansion in deep neural networks. *CoRR*, *abs/1906.00443*. Retrieved from http://arxiv.org/abs/1906.00443

Richards, B. A., Lillicrap, T. P., Beaudoin, P., Bengio, Y., Bogacz, R., Christensen, A., ... Kording, K. P. (2019, Nov 01). A deep learning framework for neuroscience. *Nature Neuroscience*, *22*(11), 1761-1770. Retrieved from https://doi.org/10.1038/s41593-019-0520-2 doi: 10.1038/s41593-019-0520-2

Ridnik, T., Baruch, E. B., Noy, A., & Zelnik-Manor, L. (2021). Imagenet-21k pretraining for the masses. *CoRR*, *abs/2104.10972*. Retrieved from https://arxiv.org/abs/2104.10972

Russakovsky, O., Deng, J., Su, H., Krause, J., Satheesh, S., Ma, S., ... Fei-Fei, L. (2015). ImageNet Large Scale Visual Recognition Challenge. *International Journal of Computer Vision (IJCV)*, *115*(3), 211-252. doi: 10.1007/s11263-015-0816-y

Saxena, S., & Cunningham, J. P. (2019, April). Towards the neural population doctrine. *Current Opinion in Neurobiology*, *55*, 103–111. Retrieved 2022-06-14, from https://linkinghub.elsevier.com/retrieve/pii/S0959438818300990 doi: 10.1016/j.conb.2019.02.002

Schrimpf, M., Kubilius, J., Hong, H., Majaj, N. J., Rajalingham, R., Issa, E. B., ... DiCarlo, J. J. (2018). Brain-score: Which artificial neural network for object recognition is most brain-like? *bioRxiv preprint*. Retrieved from https://www.biorxiv.org/content/10.1101/407007v2

Schrimpf, M., Kubilius, J., Lee, M. J., Murty, N. A. R., Ajemian, R., & DiCarlo, J. J. (2020). Integrative benchmarking to advance neurally mechanistic models of human intelligence. *Neuron*. Retrieved from https://www.cell.com/neuron/fulltext/S0896-6273(20)30605-X

Sexton, N. J., & Love, B. C. (2021, June). *Directly interfacing brain and deep networks exposes non-hierarchical visual processing* (preprint). Neuroscience. Retrieved 2022-06-24, from http://biorxiv.org/lookup/doi/10.1101/2021.06.28.450213 doi: 10.1101/2021.06.28.450213

Simoncelli, E. P., & Olshausen, B. A. (2001). Natural image statistics and neural representation. *Annu Rev Neurosci*, *24*, 1193–1216.

Smith, L. B., Jones, S. S., Landau, B., Gershkoff-Stowe, L., & Samuelson, L. (2002, January). Object name learning provides on-the-job training for attention. *Psychol Sci*, *13*(1), 13–19.

Smith Breault, M. (2020, July). *Monkey brain.* Zenodo. Retrieved from https://doi.org/10.5281/zenodo.3926117 doi: 10.5281/zenodo.3926117

Sorscher, B., Ganguli, S., & Sompolinsky, H. (2021). The geometry of concept learning. *bioRxiv*. Retrieved from https://www.biorxiv.org/content/early/2021/03/21/2021.03.21.436284 doi: 10.1101/2021.03.21.436284

Stojanoski, B., & Cusack, R. (2014, October). Time to wave good-bye to phase scrambling: creating controlled scrambled images using diffeomorphic transformations. *J Vis*, *14*(12).

Stringer, C., Pachitariu, M., Steinmetz, N., Carandini, M., & Harris, K. D. (2019, Jul 01). High-dimensional geometry of population responses in visual cortex. *Nature*, *571*(7765), 361-365. Retrieved from https://doi.org/10.1038/s41586-019-1346-5 doi: 10.1038/s41586-019-1346-5

Tishby, N., & Zaslavsky, N. (2015, March). Deep Learning and the Information Bottleneck Principle. *arXiv:1503.02406 [cs]*. Retrieved 2022-06-15, from http://arxiv.org/abs/1503.02406 (arXiv: 1503.02406)

Yamins, D. L. K., & DiCarlo, J. J. (2016, Mar 01). Using goal-driven deep learning models to

understand sensory cortex. *Nature Neuroscience*, *19*(3), 356-365. Retrieved from https://doi.org/10.1038/nn.4244 doi: 10.1038/nn.4244

Yamins, D. L. K., Hong, H., Cadieu, C. F., Solomon, E. A., Seibert, D., & DiCarlo, J. J. (2014). Performance-optimized hierarchical models predict neural responses in higher visual cortex. *Proceedings of the National Academy of Sciences*, *111*(23), 8619–8624. Retrieved from https://www.pnas.org/content/111/23/8619 doi: 10.1073/pnas.1403112111

Zamir, A. R., Sax, A., Shen, W. B., Guibas, L., Malik, J., & Savarese, S. (2018). Taskonomy: Disentangling task transfer learning. In *2018 ieee conference on computer vision and pattern recognition (cvpr)*.

Zhang, C., Bengio, S., Hardt, M., Recht, B., & Vinyals, O. (2016). Understanding deep learning requires rethinking generalization. *CoRR*, *abs/1611.03530*. Retrieved from http://arxiv.org/abs/1611.03530

Zhu, W., Qiu, Q., Huang, J., Calderbank, R., Sapiro, G., & Daubechies, I. (2018, June). LDMNet: Low Dimensional Manifold Regularized Neural Networks. In *2018 IEEE/CVF Conference on Computer Vision and Pattern Recognition* (pp. 2743–2751). Salt Lake City, UT, USA: IEEE. Retrieved 2022-06-15, from https://ieeexplore.ieee.org/document/8578388/ doi: 10.1109/CVPR.2018.00290

Zhuang, C., Yan, S., Nayebi, A., Schrimpf, M., Frank, M. C., DiCarlo, J. J., & Yamins, D. L. K. (2021). Unsupervised neural network models of the ventral visual stream. *Proceedings of the National Academy of Sciences*, *118*(3). Retrieved from https://www.pnas.org/content/118/3/e2014196118 doi: 10.1073/pnas.2014196118

Appendix A Anticipated questions

In this section, we address some questions that readers are likely to have regarding our results and conclusions. While certain parts of our responses are more speculative in nature and have yet to be tested empirically, we believe that they nevertheless provide useful insights.

Question: Isn't it trivially true that models with higher latent dimensionality will exhibit better encoding performance?

It is important to emphasize that the relationship between ED and encoding performance cannot be explained as a trivial statistical consequence of models with high ED. First, all models were evaluated using cross-validation, which means that the only way for a model to perform well is by explaining meaningful variance that generalizes to held-out data. If models with high ED were simply overfit to the training data, their performance on the held-out test data would be poor. Second, our ED metric characterizes the distribution of variance in the eigenspectrum, but it does not directly indicate the number of available dimensions in a system, nor does it change the number of parameters in the model. In fact, all models examined here were full rank, meaning that their image representations spanned the maximum number of latent dimensions. Thus, in our analyses, ED alone has no direct relationship to the maximum number of latent dimensions that could potentially be used in a regression. Finally, the data that we modeled come from a high-level visual region (IT) whose image-evoked responses have long been a challenging target for computational modelers. In fact, decades of efforts to model the representations in this brain region directly led to the advent of deep learning approaches for the computational neuroscience of vision (Kriegeskorte, 2015; Yamins et al., 2014). If any model with high ED could trivially explain the representations of IT, then neuroscientists would have no need for deep neural networks. One could, instead, solve the challenging problem of modeling IT by running linear regression on RGB pixel values and adding polynomials or interaction terms until ED was high enough to account for the variance in neural responses. The reason that such an approach would not work is that the space of all possible image representations is infinite: there is an unlimited variety of arbitrary computations that could be used to add dimensions to a model. Models that achieve high ED through arbitrary computations would have a negligible probability of overlapping with the representations of visual cortex. We, thus, suspect that the use of performance-optimized DNN architectures is critical for constraining the computations of encoding models and increasing their overlap with cortical representations.

Question: Why should we care about latent dimensionality if ImageNet classification performance also correlates with encoding performance?

Prior work has found that a model's object classification accuracy (e.g., on ImageNet) strongly correlates with its encoding performance for certain brain regions (Yamins et al., 2014; Zhuang et al., 2021). Could we simply focus on classification accuracy, or is latent dimensionality theoretically important in its own right?

While object classification accuracy seems to account for the encoding performance of current models, it is worth asking whether or not it can be a viable theory going forward. To say that it is a complete explanation is to say that we believe the correlation between classification accuracy and encoding performance will hold indefinitely, across the space of all current and future models (i.e., a model that performs better on object classification will always obtain higher encoding performance). This is unlikely to be the case. Optimal object classification requires that a model be invariant to features unrelated to object identity, such as orientation and position, which can only contribute to noise in the classifier (Recanatesi et al., 2019). However, we know that the brain represents orientation, position, and a host of other features unrelated to object identity. Therefore, we know that the object classification theory of encoding performance breaks down in some regime, and that the true dimensionality of visual cortex must be higher than what ideal object classification models would predict. Indeed, initial results suggest that the relationship between object classification and encoding performance does indeed break down past a certain ImageNet classification accuracy (Schrimpf et al., 2018, 2020). A theory based on latent dimensionality (and alignment pressure) has the potential to explain the encoding performance of both current and future models on more rich neural datasets, and it may help us to understand why the relationship between encoding performance and classification accuracy breaks down at the highest levels of classification performance.

An interesting question emanating from this discussion is whether the observed relationship between classification accuracy and encoding performance might be overly optimistic due to the limited space of DNNs that are available for computational neuroscientists to examine. Most of the DNNs in visual neuroscience are trained on ImageNet or similar image databases, and we do not have DNNs that can perform open-ended tasks in complex, real-world environments. If we did have DNNs that handled more complex and naturalistic visual behaviors, we postulate that they would surpass the encoding performance of our best object-classification models (and also have higher dimensionality). With the current space of state-of-the-art DNNs being dominated by (a) supervised object classification and (b) self-supervised objectives that learn invariances tailored to object classification, we are bound to observe the current correlation between object classification performance and encoding performance because object recognition is undoubtedly *one* important problem that biological vision solves—but, importantly, it is one of *many* complex problems solved by the representations of visual cortex.

Question: Does effective dimensionality really represent the number of accurately encoded visual features?

Essential to our theory is the assumption that the variance of a representation along a particular dimension is proportional to the meaningfulness of the feature it encodes. In such cases, it is valid to say that ED roughly quantifies the number of encoded visual features. This interpretation is central to popular dimensionality reduction techniques, such as PCA, and it has good theoretical support given that high-variance dimensions are typically more robust and would, thus, be best-suited for carrying the signal in a population code. Importantly, in the DNN literature, recent findings have shown that neural networks expand variance along dimensions that are useful for solving their tasks and contract variance along noise dimensions that are left over from their random initialization (Flesch et al., 2022; Frei et al., 2022; Recanatesi et al., 2019). There is, thus, a straightforward relationship between the number of meaningful latent dimensions in a neural network and the shape of the principal component variance spectrum.

Nonetheless, there is no guarantee that high-variance dimensions correspond to meaningful signal and that low-variance dimensions correspond to random features or noise. Furthermore, ED is only an imperfect summary statistic of the rate of decay of the eigenspectrum, and does not directly quantify the number of meaningful features features. An interesting direction for future work would be the development of dimensionality metrics that try to explicitly differentiate between meaningful and random dimensions in DNNs, as can be done for neural data when using repeated stimulus presentations (Stringer et al., 2019).

Appendix B Theory of latent dimensionality and encoding performance

While the space of all possible visual stimuli is vast and high-dimensional, we can define many lower-dimensional subspaces within it, referred to as *subspaces* B.1a. For instance, the *natural image subspace* consists solely of images taken from the physical world, and typical neuroscience experiments consist of tightly controlled stimulus sets spanning a *data subspace*. In a similar way, we can formalize visual representations and the features they encode using the framework of subspaces embedded in a higher-dimensional visual space.

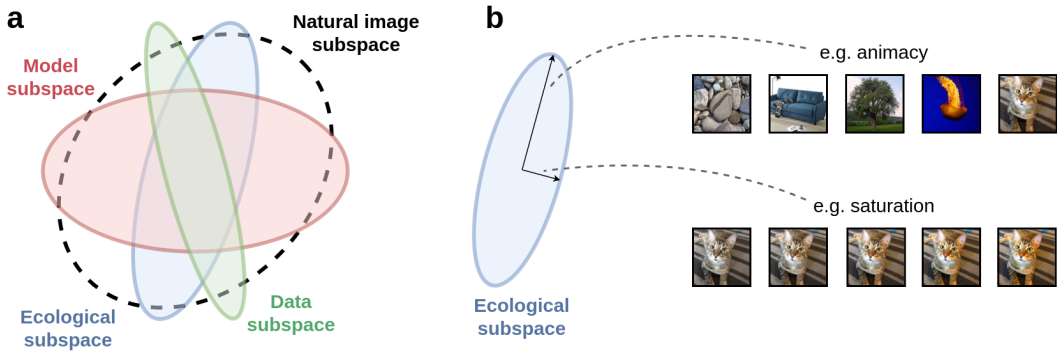

Figure B.1: A theory of latent dimensionality and encoding performance. a. Our theory models the distribution of natural images, the distribution of experimental stimuli, and the features encoded by brains and models as lower-dimensional subspaces embedded in a high-dimensional ambient space (denoted here using ellipses of varying eccentricity). **b.** For ecological and model subspaces, the variance along a dimension represents the accuracy with which it is encoded. For example, visual cortex might accurately encode differences in animacy (high variance), but only coarsely encode differences in color saturation (low variance).

For instance, if we were to show a human subject a set of object images that varied along the dimension of animacy (e.g., ranging from inanimate rocks to cats) we would expect them to clearly and accurately notice the differences between these images (see Figure B.1b). On the other hand, if we were to vary a more perceptually subtle property, such as color saturation, the differences might appear less pronounced and we could say that the visual system is less accurate along this dimension. At the extreme, we could generate images by sampling from a distribution of white noise, in which case differences would be almost imperceptible, despite varying significantly in the input space.

What these examples show is that the human brain does not accurately encode the vast space of all possible visual dimensions, but only a lower-dimensional subspace of these dimensions that are ecologically relevant for survival and behavior in the real world (i.e., dimensions along an *ecological subspace*). In the same way, any computational model of perception, such as a DNN, will preferentially encode different visual dimensions more or less accurately and define its own representational *model subspace*. We refer to dimensions along these representational subspaces as *latent*, and we refer to the dimensions of the larger visual space in which they are embedded as *ambient*.

With these concepts in mind, we can now begin to think about the conditions under which a model can achieve high encoding performance when predicting a given neural dataset. Intuitively, this can only happen when the stimuli span dimensions that are accurately encoded by *both* the model and the brain. In other words, the latent dimensions of the ecological subspace must overlap with latent dimensions of the model subspace. A key factor driving our simulated and empirical results is that the probability of these overlaps increases substantially as the latent dimensionality of the model subspace grows.

Appendix C Implementation of simulations

Our process is summarized in Figure C.1, and consists of 3 steps. First, given our simulation parameters, we sampled subspace geometries within a high-dimensional ambient space. Next, we generated a set of experimental stimuli from the data subspace and projected them onto both the ecological and model subspaces, yielding a set of neural and model activations. Finally, we fit a linear encoding model to measure how well neural responses to the stimuli could be predicted from the corresponding model activations. By repeating this process across a range of simulation parameters (e.g., different model effective dimensionalities), we could better understand their influences on encoding performance. We describe this process in more detail below.

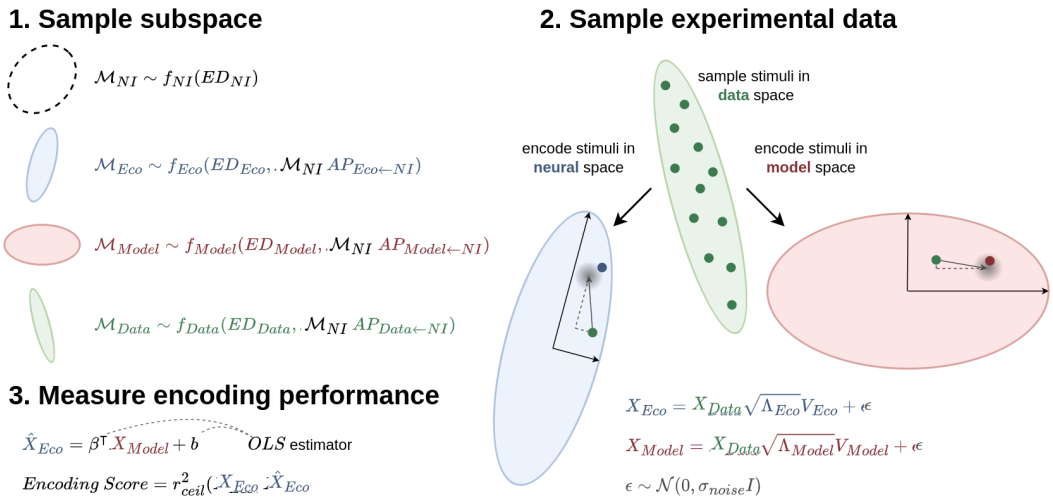

Figure C.1: Simulating our theory of latent dimensionality and encoding performance. 1. Our Gaussian subspaces were sampled to have a desired effective dimensionality. The ecological, model, and data subspaces were also sampled with a given alignment pressure to a shared space: the natural image subspace. **2.** Experimental data were sampled from the distribution specified by the experimental data subspace and then projected onto the ecological and model subspaces, which stretch or compress the data according to their variance along different dimensions. Isotropic noise was then added so that high-variance subspace dimensions had higher SNR and more accurately encoded their corresponding image features. **3.** A linear encoding model was trained using ordinary least squares (OLS) regression to predict neural responses from model activations. The reported encoding score is the percentage of explained variance normalized to the noise-ceiling of the neural data.

subspace geometry In essence, our simulations consider four subspaces and relations between them: the natural image subspace, the data subspace from which experimental stimuli are sampled, the ecological subspace governing neural representations, and the model subspace. For simplicity, we parameterized all subspaces as multivariate Gaussian distributions embedded in a common ambient space of all possible visual dimensions. Using multivariate Gaussians also provided a simple method for modulating and measuring the subspace's latent dimensionality, which we describe later in this section.

Variance along latent dimensions In our simulations, the amount of variance in a subspace along a given dimension has important significance. For the natural image and data subspaces, this variance corresponds to changes in a particular image feature (e.g., animacy). For the ecological and model representational subspaces, however, the variance along a dimension represents how accurately that dimension is encoded by the brain or a particular model. For example, consider Figure B.1b. Here, the human brain accurately and precisely represents differences in object animacy (high-variance dimension) but is relatively imprecise in how it represents fine changes in color saturation (low-variance dimension). One way to re-frame this idea is to think of the variance along a given dimension as representing its signal-to-noise-ratio (SNR).

Sampling subspaces Within an image space of ambient dimensionality D_a, we wished to generate multivariate Gaussian subspaces with desired effective dimensionalities and mutual alignment pressures (Figure C.1 step 1). First, we sampled a natural image subspace $\mathcal{M}_{NI}$ with effective dimensionality ED_{NI}. The orthonormal eigenvectors for this subspace were sampled uniformly within the ambient dimensional space, whereas the eigenvalues were selected deterministically to achieve ED_{NI}. Although there are many ways to design eigenspectra with a particular ED, we opted to parameterize the decay rate of the eigenvalues as a power law $\lambda_i = \frac{1}{i^\alpha}$ and solved for the α that yielded our desired ED.

We next sampled the ecological subspace $\mathcal{M}_{Eco}$, model subspace $\mathcal{M}_{Model}$, and data subspace $\mathcal{M}_{Data}$. To select their eigenvalues, we followed the same power law parameterization as for the natural image subspace to achieve effective dimensionalities ED_{Eco}, ED_{Model}, and ED_{Data}. Their eigenvectors, however, were all sampled in a way that depended on their respective alignment pressures to the natural image subspace $AP_{Eco \leftarrow NI}$, $AP_{Model \leftarrow NI}$, and $AP_{Data \leftarrow NI}$. This aspect of the sampling procedure is described in detail below.

Formulation of AP In our simulations, AP is a scalar value that ranges between -1 and 1. An $AP = 0$ corresponds to no alignment pressure, in which case a basis of eigenvectors is sampled uniformly in the ambient space. When $AP > 0$, eigenvectors are sampled such that dimensions with larger eigenvalues capture more of the total variance in the natural image subspace (i.e., the high-variance dimensions of both subspaces are more likely to be aligned). On the other hand, when $AP < 0$, eigenvectors are sampled to preferentially align with low-variance dimensions of the natural image subspace.

Specifically, we needed to sample orthogonal vectors to form the eigenbasis of a new Gaussian subspace $\mathcal{M}_a$, where those vectors preferentially spanned regions of high-variance in a reference Gaussian subspace $\mathcal{M}_b$, in a way that depended on $AP_{a \leftarrow b}$. We achieved this by first defining a multivariate Gaussian distribution $\mathcal{N}_{a \leftarrow b}(0, \Sigma_{a \leftarrow b})$. The eigenvectors of $\Sigma_{a \leftarrow b}$ were equal to those of $\mathcal{M}_b$, while the eigenvalues of $\Sigma_{a \leftarrow b}$ were generated as follows:

$$x_i = \begin{cases} \frac{i-1}{D_a - 1}, & \text{if } AP_{a \leftarrow b} \in [0, 1] \\ \frac{1-i}{D_a - 1}, & \text{if } AP_{a \leftarrow b} \in [-1, 0) \end{cases} \tag{1}$$

$$\lambda_i = e^{-s AP_{a \leftarrow b} x_i} \tag{2}$$

where i is the index of the eigenvalue starting from 1, D_a is the ambient dimensionality of the subspaces, and s is a scaling factor which we set to 20. Essentially, this drew eigenvalues from D_a equally spaced points on an exponential function in the domain of [0, 1] that is either decaying (in the case of positive AP) or growing (in the case of negative AP).

Next, we iteratively (1) sampled a vector $v_i \sim \mathcal{N}^{(i)}_{a \leftarrow b}$, (2) normalized v_i to unit length, and (3) projected $\mathcal{N}^{(i)}_{a \leftarrow b}$ onto the subspace orthogonal to v_i, giving $\mathcal{N}^{(i+1)}_{a \leftarrow b}$. This process was repeated D_a times. We then used the normalized v_i's as the eigenvectors of M_a. First, note that the v_i's collectively define an orthonormal basis because each is sampled from a subspace orthogonal to $v_{1:i-1}$. Second, note that for positive $AP_{a \leftarrow b}$ early v_i's are more likely to be oriented towards regions of high variance in M_b, where $\mathcal{N}_{a \leftarrow b}$ has most of its probability mass. For negative $AP_{a \leftarrow b}$, though, the probability mass of $\mathcal{N}_{a \leftarrow b}$ is concentrated along low-variance dimensions in M_b, which results in early v_i's that tend to point in low-variance dimensions of M_b as well. For an $AP_{a \leftarrow b} = 0$, the covariance matrix of $\mathcal{N}_{a \leftarrow b}$ is identity, and the v_i's thus do not depend on the eigenvectors of M_b in any way. Collectively, these properties satisfied our desiderata regarding the function of alignment pressure.

Sampling experimental data Having generated subspaces that specified the distribution of stimuli as well as model and ecological coding properties, our next step was to sample experimental data (Figure C.1 step 2). First, we sampled N points from the multivariate Gaussian distribution specified by the data subspace:

$$x_i^{Data} \sim \mathcal{N}(0, V_{Data} \Lambda_{Data} V_{Data}^T) \tag{3}$$

where V_{Data} denotes the column matrix of data subspace eigenvectors and Λ_{Data} is the diagonal eigenvalue matrix. These points can be thought of as experimental stimuli, which vary along different image dimensions.

Next, we projected the stimuli onto the eigenvectors of both the ecological and model subspaces (V_{Eco} and V_{Model}) and scaled them by the standard deviation along each of those eigenvectors ($\sqrt{\Lambda_{Eco}}$ and $\sqrt{\Lambda_{Model}}$). The net effect of this scaling was that the ecological/model subspaces amplified or attenuated different stimulus dimensions depending on whether or not they had significant variance along them. However, only applying this scaling would have had no effect on linear encoding performance, since regression weights could re-scale to

compensate. Therefore, after performing this projection and scaling, we added ambient noise $\epsilon \sim \mathcal{N}(0, \sigma_{noise} I)$ across all dimensions. The final result was a dataset of neural and model activations:

$$X_{Eco} = X_{Data}\sqrt{\Lambda_{Eco}}V_{Eco} + \epsilon \tag{4}$$

$$X_{Model} = X_{Data}\sqrt{\Lambda_{Model}}V_{Model} + \epsilon \tag{5}$$

Since the magnitude of the noise was equal in all directions, its net effect was to modulate the SNR along the subspace dimensions. Essentially, ecological/model dimensions with high variance were relatively unaffected by the noise and accurately encoded stimulus features, whereas dimensions with low variance were dominated by the noise and only coarsely encoded stimulus features (e.g., the ordering of different stimuli along noise-dominated dimensions might not be preserved).

Measuring encoding performance After having stimulated neural and model activations, our last step was to measure the linear encoding performance of predicting X_{Eco} from X_{Model}. Specifically, we predicted neural activations $\hat{X}_{Eco}$ and then computed the percentage of explained variance normalized to the noise ceiling of X_{Eco}:

$$\hat{X}_{Eco} = \beta X_{Model} + b \tag{6}$$

$$Encoding\ Score = r^2_{ceil}(X_{Eco}, \hat{X}_{Eco}) \tag{7}$$

where the regression parameters β and b were estimated using ordinary least squares regression without any regularization and prediction accuracy was computed through cross-validation. The noise ceiling corresponded to the percentage of variance in X_{Eco} that was explainable signal. In our simulations, we had direct access to this value because E_{Eco} was generated according to:

$$X_{Eco} = X_{Data}\sqrt{\Lambda_{Eco}}V_{Eco} + \epsilon \tag{8}$$

$$= X^{(signal)}_{Eco} + \epsilon \tag{9}$$

where $X^{(signal)}_{Eco}$ is the signal component of X_{Eco}. Thus, we simply fit another linear regression model to predict X_{Eco} using $X^{(signal)}_{Eco}$ as regressors, in which case the resulting percentage of explained variance r^2 corresponded to the noise ceiling.

When computing percentages of explained variance, we also needed to aggregate across all dimensions (i.e., neurons) of X_{Eco} that were predicted. Typically, this is done by taking the mean r^2_i across all dimensions i, but this would violate an important principal of our theory wherein dimensions with larger variance contain more signal, and are therefore more important to predict. Instead, we computed a weighted average of all r^2_i, with weights equal to the variance in X_{Eco} along dimension i.

Simulation parameters Unless otherwise stated, our simulation parameters were set as follows: $D_a = 100$, $ED_{NI} = 20$, $ED_{Eco} = 10$, $ED_{Data} = 100$, $AP_{Eco \leftarrow NI} = 0.75$, $AP_{Model \leftarrow NI} = 0.75$, $\sigma_{noise} = 0.1$. ED_{Model} ranged from 1 to D_a, and 50 repeats of the simulation were performed for all values of ED_{Model}, each with independently sampled subspaces/datasets.

Appendix D Additional simulation results

In this section, we show how the relationship between ED_{Model} and encoding performance can be modulated by different settings of ED_{Eco}, AP, and σ_{noise}. Figure D.1 demonstrates these effects, which we interpret below.

Increasing ED_{Eco} As ED_{Eco} increased, higher ED_{Model} was needed to achieve the same level of encoding performance simply because there were more ecological dimensions to explain. In practice, this means that if the ecological subspace (i.e., representations in visual cortex) is high-dimensional, encoding performance will saturate later as a function of ED_{Model}.

Increasing AP In regards to different AP between the model and ecological subspaces to the natural image subspace, we see that lower-dimensional models were able to achieve better encoding performance if they were preferentially aligned to ecological dimensions. Nevertheless, given any constant alignment pressure, there remains a positive correlation between ED_{Model} and encoding performance, indicating independent contributions.

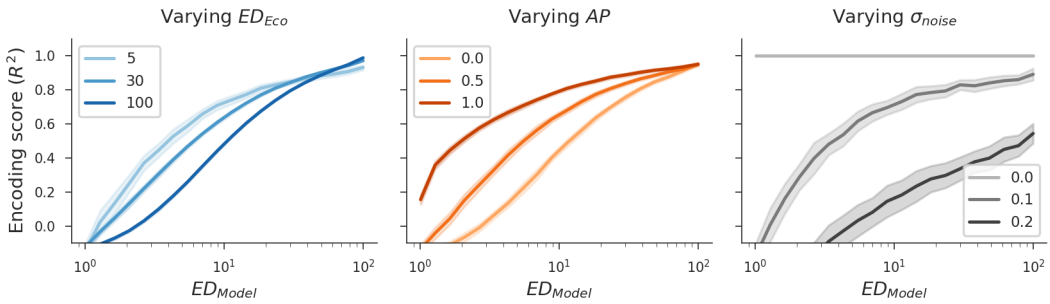

Figure D.1: Modulating additional simulation parameters. Each simulation parameter modulated the relationship between ED_{Model} and encoding performance. Within a plot, only the titled parameter was changed (shown in different line colors), while other parameters were held constant.

Increasing σ_{noise} Varying σ_{noise} is key to simulations of our theory. In the case of no noise ($\sigma_{noise} = 0$), encoding performance was in fact independent of ED_{Model}, and all models achieved perfect encoding performance. This is because our models had *some* non-zero variance along every ambient dimension, which, in the absence of noise, always led to an SNR of ∞. In essence, the variance along a dimension had no semantic meaning in this case because it could be scaled arbitrarily without any change in the representation. As σ_{noise} increased, however, having high variance along a dimension became increasingly more important for accurately representing features with high SNR, and encoding performance therefore became more dependent on high ED_{Model}.

Limitations of our theory and simulations While our simulations provide valuable intuitions regarding ED, AP, and encoding performance, they make several simplifying assumptions that are unlikely to hold in practice. First, they assume that all subspaces are multivariate Gaussians, in which case linear metrics such as ED are appropriate for estimating latent dimensionality. While the precise topologies of subspaces in biological and artificial neural representations are unknown, there is evidence that they are likely nonlinear (Ansuini et al., 2019). Another simplification is that our simulations sample linear model and neural dimensions within the *same* ambient space, whereas in reality models and the brain both nonlinearly transform image dimensions. In other words, an image feature that is linearly encoded in the ecological subspace might be highly curved and warped in the model subspace. Future work could build on our simulation framework to explore these issues.

Appendix E Details of DNN models

Table E.1 lists details for all DNNs used in our experiments. *PyTorch* models were obtained from the torchvision package and from PyTorch Hub (Paszke et al., 2019), *VVS* models were obtained from Zhuang et al. (2021), and *Taskonomy* models were obtained from Zamir et al. (2018).

Table E.1: DNN models used in experiments

Training task	Learning setting	Training dataset	Architecture	Source
Object classification	Supervised	ImageNet	ResNet18	PyTorch
Object classification	Supervised	ImageNet	ResNet50	PyTorch
Barlow-Twins	Self-Supervised	ImageNet	ResNet50	PyTorch
N/A	Untrained	N/A	ResNet18	N/A
N/A	Untrained	N/A	ResNet50	N/A
Object classification	Supervised	ImageNet	ResNet18	VVS
Depth prediction	Supervised	ImageNet	ResNet18	VVS
Auto-encoding	Self-supervised	ImageNet	ResNet18	VVS
Colorization	Self-supervised	ImageNet	ResNet18	VVS
Contrastive multiview coding	Self-supervised	ImageNet	ResNet18	VVS
Contrastive predictive coding	Self-supervised	ImageNet	ResNet18	VVS
Deep cluster	Self-supervised	ImageNet	ResNet18	VVS
Instance recognition	Self-supervised	ImageNet	ResNet18	VVS
Local aggregation	Self-supervised	ImageNet	ResNet18	VVS
Relative position	Self-supervised	ImageNet	ResNet18	VVS
SimCLR	Self-supervised	ImageNet	ResNet18	VVS
Object classification	Supervised	Indoor buildings	ResNet50	Taskonomy
Scene classification	Supervised	Indoor buildings	ResNet50	Taskonomy
Semantic segmentation	Supervised	Indoor buildings	ResNet50	Taskonomy
Curvature estimation	Supervised	Indoor buildings	ResNet50	Taskonomy
Depth estimation	Supervised	Indoor buildings	ResNet50	Taskonomy
Depth estimation (z-buffer)	Supervised	Indoor buildings	ResNet50	Taskonomy
Edge detection (2D)	Supervised	Indoor buildings	ResNet50	Taskonomy
Edge detection (3D)	Supervised	Indoor buildings	ResNet50	Taskonomy
Egomotion	Supervised	Indoor buildings	ResNet50	Taskonomy
Fixated pose estimation	Supervised	Indoor buildings	ResNet50	Taskonomy
Non-fixated pose estimation	Supervised	Indoor buildings	ResNet50	Taskonomy
Keypoint detection (2D)	Supervised	Indoor buildings	ResNet50	Taskonomy
Keypoint detection (3D)	Supervised	Indoor buildings	ResNet50	Taskonomy
Point matching	Supervised	Indoor buildings	ResNet50	Taskonomy
Reshading	Supervised	Indoor buildings	ResNet50	Taskonomy
Room layout estimation	Supervised	Indoor buildings	ResNet50	Taskonomy
Surface normal estimation	Supervised	Indoor buildings	ResNet50	Taskonomy
Vanishing point estimation	Supervised	Indoor buildings	ResNet50	Taskonomy
Auto-encoding	Self-supervised	Indoor buildings	ResNet50	Taskonomy
Denoising	Self-supervised	Indoor buildings	ResNet50	Taskonomy
Inpainting	Self-supervised	Indoor buildings	ResNet50	Taskonomy
Jigsaw	Self-supervised	Indoor buildings	ResNet50	Taskonomy
Unsupervised segmentation (2D)	Self-supervised	Indoor buildings	ResNet50	Taskonomy
Unsupervised segmentation (2.5D)	Self-supervised	Indoor buildings	ResNet50	Taskonomy

Appendix F Additional analyses of ED and encoding performance

Here, we replicate our results in more contexts. Figure F.1 shows the relationship between effective dimensionality and encoding performance without applying a max-pooling operation to the DNN feature maps. Figures F.2 and F.3 shows encoding performance across multiple species, recording modalities, and brain regions. Figure F.4 fits encoding models using OLS instead of partial-least-squares regression.

Our general results hold across all of these settings, with the exception of V1 in the monkey electrophysiology data. We speculate that this is due to the far lower complexity of representations in V1, which serve primarily as simple edge detectors for later processing in higher-level regions.

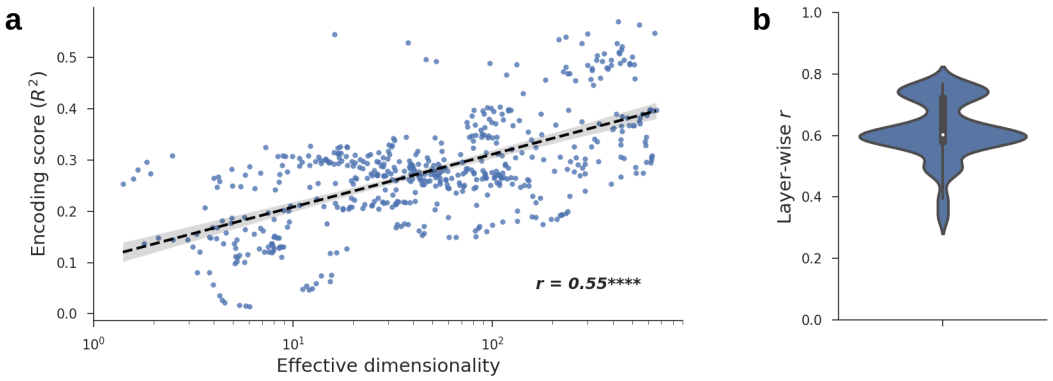

Figure F.1: Effective dimensionality and encoding performance without max-pooling. a. The encoding performance achieved by a model scaled with the effective dimensionality of its entire feature map (without max-pooling applied). Each point in the plot was obtained from one layer from one DNN, resulting in a total of 536 models (see main text for further details). **b.** Even when conditioning on a particular DNN layer, controlling for both depth and ambient dimensionality, effective dimensionality and encoding performance continued to strongly correlate. The plot shows the distribution of these correlations (Pearson r) across all unique layers in our analyses.

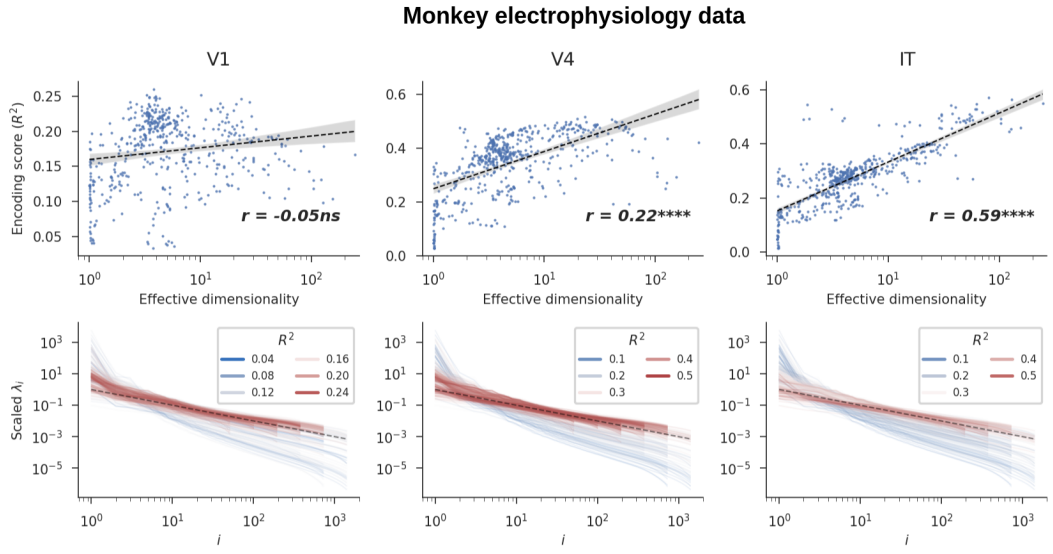

Figure F.2: Latent dimensionality and encoding performance on monkey electrophysiology data. The encoding performance for all of our models across multiple brain regions in monkey electrophysiology datasets collected by Majaj et al. (2015) (IT and V4) and Freeman et al. (2013) (V1), plotted against the models' ED and eigenspectra. Our results hold across all brain regions except for V1; encoding performance increases with latent dimensionality.

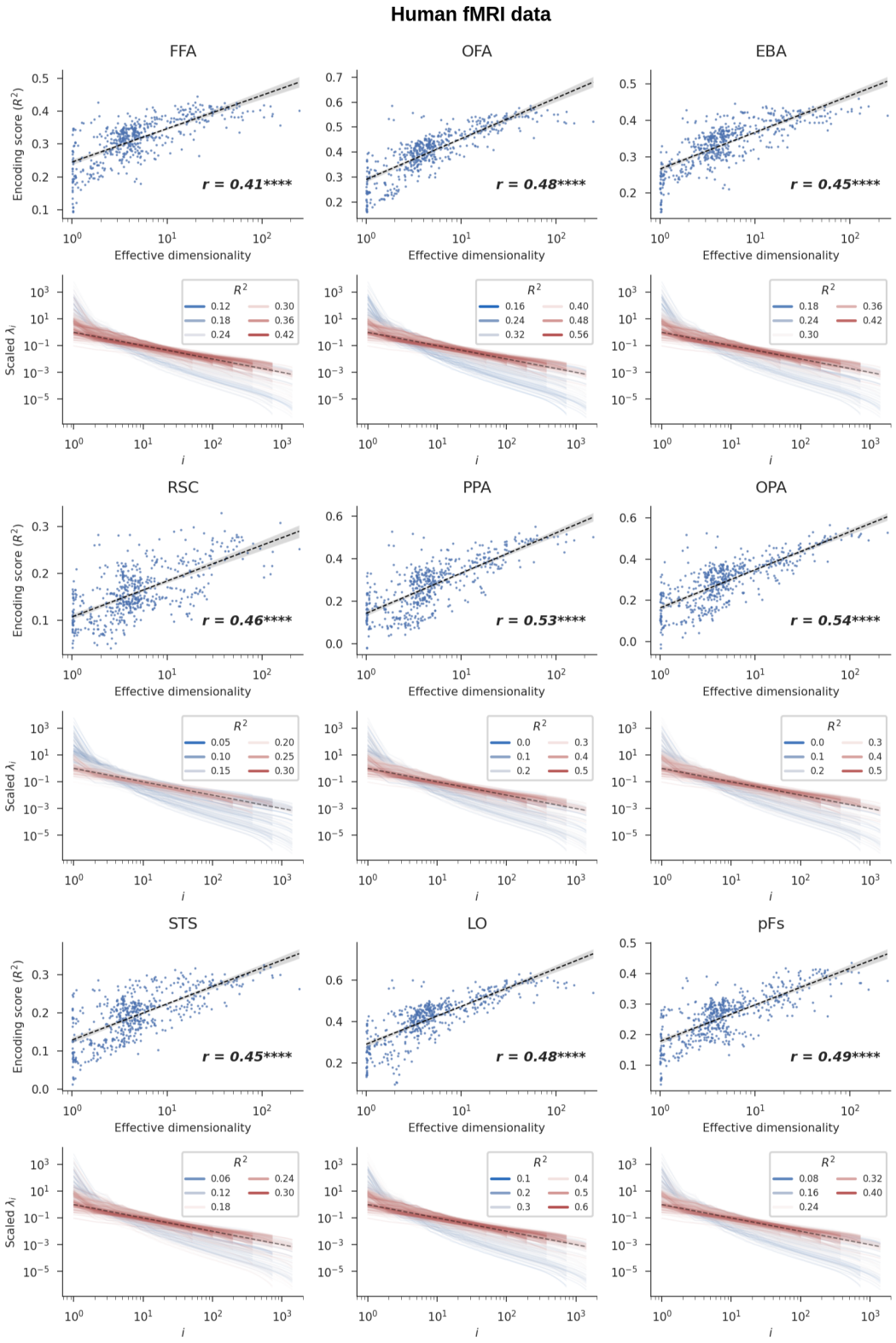

Figure F.3: Latent dimensionality and encoding performance on human fMRI data. The encoding performance for all of our models across multiple brain regions in a human fMRI dataset collected by Bonner and Epstein (2021), plotted against the models' ED and eigenspectra. Our results hold across all brain regions; encoding performance increases with latent dimensionality. FFA=fusiform face area, OFA=occipital face area, EBA=extrastriate body area, RSC=retrosplenial complex, PPA=parahippocampal place area, OPA=occipital place area, STS-superior temporal sulcus, LO=lateral occipital region, pFs=posterior fusiform region.

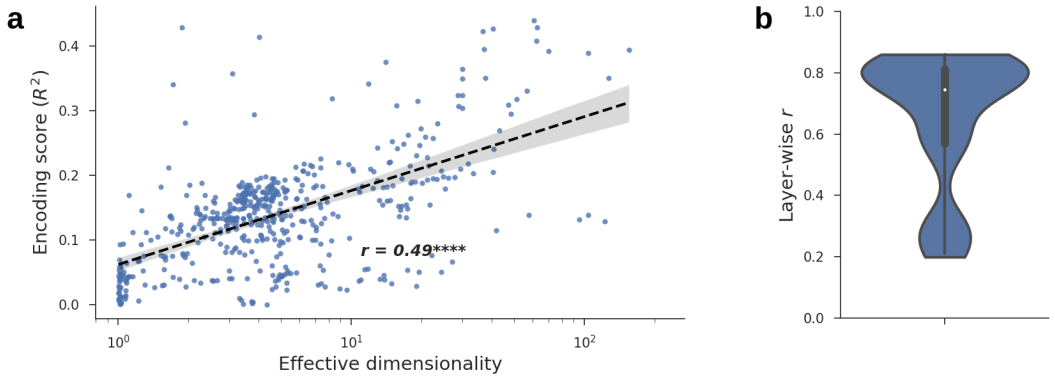

Figure F.4: Effective dimensionality and encoding performance using OLS regression. a. The encoding performance achieved by a model fit using OLS regression scaled with its effective dimensionality. Each point in the plot was obtained from one layer from one DNN, resulting in a total of 536 models (see main text for further details). **b.** Even when conditioning on a particular DNN layer, controlling for both depth and ambient dimensionality, effective dimensionality and encoding performance continued to strongly correlate. The plot shows the distribution of these correlations (Pearson r) across all unique layers in our analyses.

Appendix G ED and Representational Similarity Analysis

To provide additional evidence that our central results are not due to trivial statistical effects wherein models with higher latent dimensionality have more degrees of freedom to predict neural data, we replicated our results using Representational Similarity Analysis (RSA) (Kriegeskorte et al., 2008). In representational similarity analysis, a dissimilarity matrix is constructed for both the model and the brain data by computing a distance between the representations for each pair of stimuli. These matrices are then correlated to evaluate their similarity. Importantly, unlike when fitting encoding models, this method for measuring the similarity between a model and the brain is entirely non-parametric and thus cannot be biased to favour models with high latent dimensionality.

While not as strong, there is nevertheless a clear trend in which models with higher RSA scores tend to have higher ED. Thus, our core results replicate using RSA.

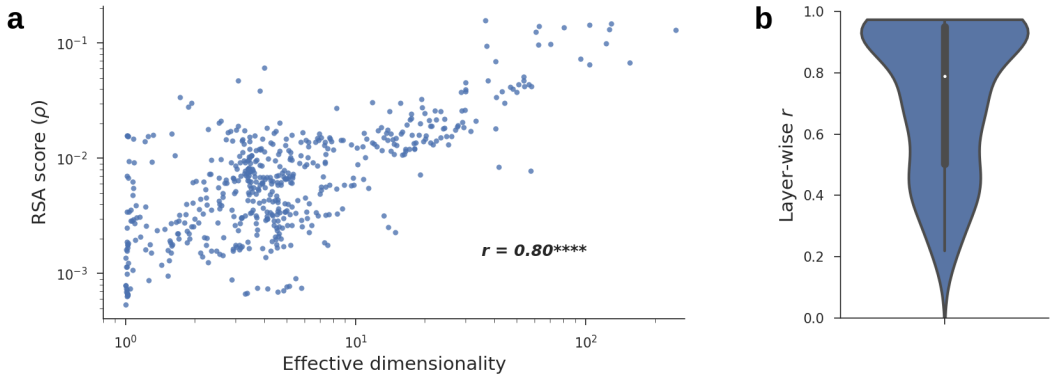

Figure G.1: Effective dimensionality and Representational Similarity Analysis (RSA). We compared the representations in our models to those in the monkey IT electrophysiology data using RSA. Note that the y-axis is on a log-scale in order to provide better resolution in face of the high variation in RSA scores. Our results hold across this different similarity metric; the similarity between model and brain representational dissimilarity matrices increases with latent dimensionality.

Appendix H ED varies with model and training parameters

To better understand how and why latent dimensionality varies in DNNs (and perhaps manipulate it for a desired effect), we can start by observing its empirical relationship to parameters of the training procedure, dataset, and architecture. Figure H.1 illustrates several of these relationships, which we were able to quantify thanks to the use of our large bank of models. We summarize our most important conclusions from these analyses below.

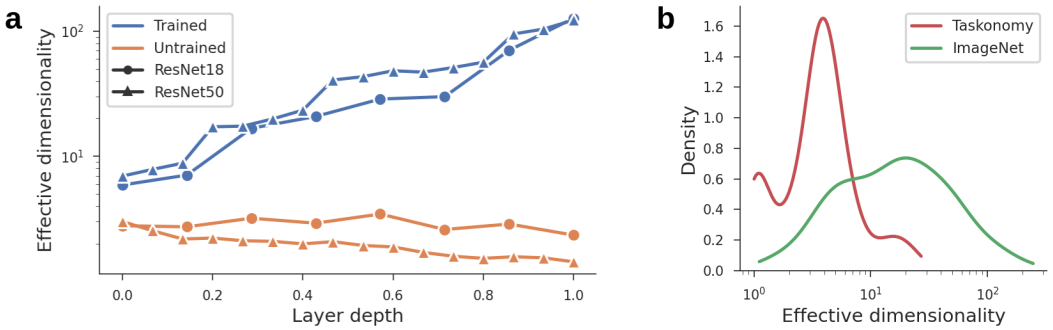

Figure H.1: Effective dimensionality varies with model and training parameters. a. Models trained on object classification (blue) had larger effective dimensionality than untrained models (orange) across all layers in ResNet18 and ResNet50. After training, effective dimensionality also gradually increased as a function of layer depth (only convolutional layers are shown). **b.** Plots indicate the distribution of effective dimensionality across models that were trained on Taskonomy (red) and ImageNet (green). These distributions differed significantly, despite the models in both groups largely sharing similar architectures and training tasks.

Training increases effective dimensionality Figure H.1a shows how effective dimensionality varied across the layer hierarchy for ResNet18 and ResNet50 architectures when they were trained on ImageNet object classification compared to when they were untrained and had randomly initialized weights. We can see that training resulted in substantial increases in effective dimensionality for both architectures across all layers. To solve complex tasks such as object classification, then, it appears that models must learn to extract a large number of orthogonal image features. This finding contradicts a commonly held belief that DNNs trained on visual tasks compress high-dimensional inputs to a small number of latent dimensions (Ansuini et al., 2019; Chung et al., 2018; Feng et al., 2022; Kingma & Welling, 2013; Recanatesi et al., 2019).

Effective dimensionality increases with layer depth Another notable trend in Figure H.1a is that effective dimensionality increased as a function of layer depth within the two supervised classification models we considered. Importantly, this cannot be explained simply as a result of an increasing number of channels along the layer hierarchy, as effective dimensionality remained more or less constant within the untrained models. This gradual increase in effective dimensionality appears to contradict other findings from (Ansuini et al., 2019; Chung et al., 2018; Cohen et al., 2020) in which latent dimensionality generally decreases as a function of layer depth, but there are important methodological differences to note. First and foremost, we computed effective dimensionality only along the channel dimension of our feature maps after applying a max-pooling operation across the spatial dimensions, which allowed us to focus on the diversity of image features. Given that spatial resolution decreases as a function of layer depth in our architectures (and most convolutional DNNs in general), the effective dimensionality of earlier layers will be higher simply due of the larger number of spatial dimensions that they contain. Another important difference in our work is that we only considered convolutional layers and performed no analyses on fully-connected layers. Indeed, much of the drop in latent dimensionality reported in other work occurs within these fully-connected layers.

Training data has a large impact on effective dimensionality Another important factor that has a significant impact on a model's learned representations is the training dataset. Our bank of models includes DNNs trained on ImageNet and Taskonomy. Figure H.1b shows the distribution of effective dimensionality for all models trained on each of these datasets. Despite similar architectures and training tasks used on both datasets, the ImageNet-trained models tended to have significantly larger effective dimensionality. Although we did not perform further analyses to determine which dataset differences explain this result, we speculate that it is due to the much greater diversity of image statistics within ImageNet. Whereas ImageNet contains images spanning many object categories appearing in diverse environments, Taskonomy consists solely of man-made indoor scenes across 600 buildings. Effective dimensionality, therefore, might scale in proportion to the complexity and variation of image features in the training data.

Appendix I Recruitment of low-variance dimensions in encoding models

The main findings that we presented in Section 2.2 contain a small number of outliers: encoding models that have low ED but nevertheless attain good encoding performance. These models are shown in Figure I.1a, along with performance-matched high-ED models for comparison. We tested the hypothesis that these outliers encode a larger number of meaningful dimensions than their low ED suggests. To do so, we examined how their encoding scores scaled as an increasing number of PCs were included as regressors. If their low-variance PCs do not

encode meaningful information, we should expect their encoding scores to saturate early on as a function of the number of PCs used.

For each model, we projected stimulus responses onto PCs computed from the ImageNet validation set (Russakovsky et al., 2015). This was done according to the same procedure that we used to calculate the ED of the models (see Materials and Methods). We then fit encoding models using responses along an increasing number of PCs as regressors. Encoding models were fit using cross-validated partial-least-squares regression and OLS regression as outlined in Materials and Methods, with a notable exception being that the PCA dimensionality reduction procedure that is described there was no longer necessary given that the regressors already consist of PCs. We used OLS in addition to partial-least-squares in order to more easily tease apart the effects of regularization when performing PCA regression.

The result of this analysis is shown in Figures I.1b (partial-least-squares regression) and I.1c (OLS regression). Despite having significantly lower ED, the outlier models continued to benefit from additional PCs at the same rate as control models that had high ED, whereas other low-ED models benefited less from adding additional PCs. Thus, unlike the other models in our analyses, it appears that the rapid decay of the eigenspectra for these outlier models does not accurately reflect the number of meaningful dimensions that they encode.

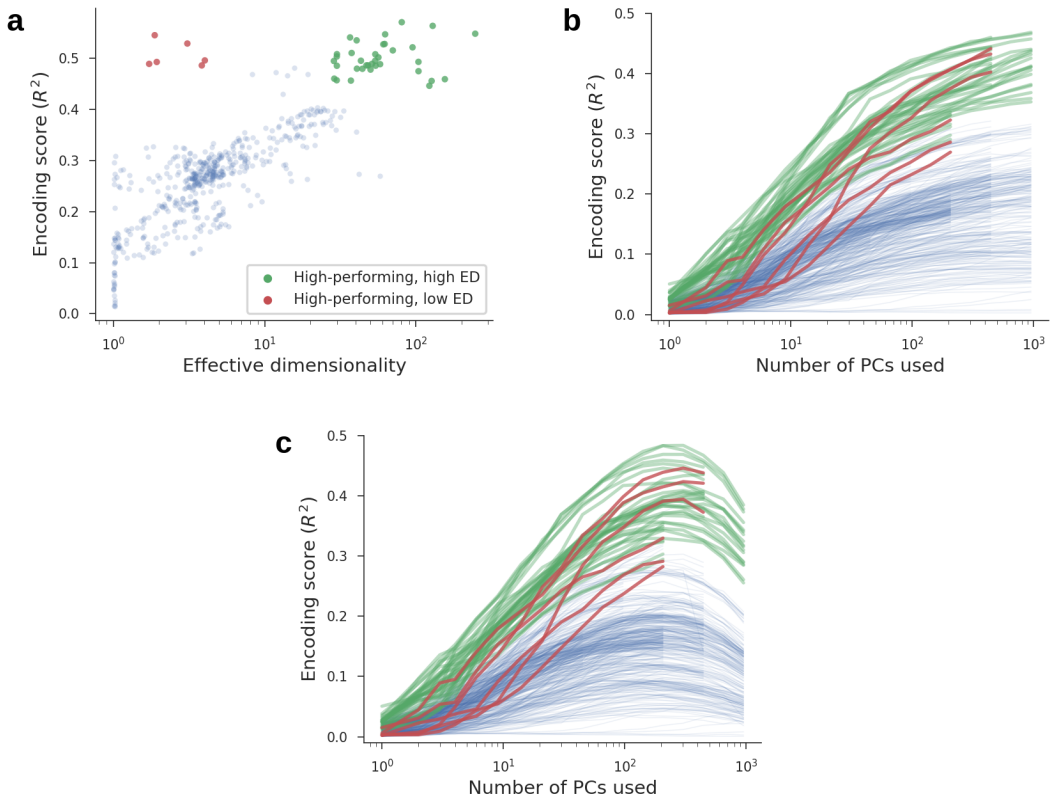

Figure I.1: Low-ED outliers still benefit from low-variance PCs. a. Among the encoding models we investigated, we observed high-performing models with high ED that fit the general trend (green samples), high-performing models with low ED that were outliers (red samples), and all other models (blue samples). **b.** We compared the degree to which these groups of encoding models benefited when an increasing number of PCs were used as regressors. Overall, encoding performance increases significantly as a function of the number of PCs used in the high-performing groups (green and red), and there is little qualitative difference between them. Importantly, both the low-ED outlier models (red) and the high-ED models (green) obtain relatively large gains in encoding performance for high-rank PCs. In contrast, the rate of increasing performance drops off more quickly for the remaining models (blue), especially for the later PCs. **c.** Same as (b), but using OLS regression to fit the encoding models. For OLS, performance drops off after about 2000 PCS because the number of features is approaching the number of training stimuli and causing overfitting (OLS is unregularized). Note that these PCs were generated from max-pooled DNN feature maps in order to match the dimensions from our ED computations, whereas the encoding models in panel (a) were fit without max-pooling and thus attained a higher encoding score. Curves for each model terminate at different locations because models differ in their ambient dimensionality, which determines their total number of PCs.

Appendix J High ED alone is not sufficient to yield strong performance

Our findings show that ED is positively correlated with encoding performance when examining standard DNNs used in computational neuroscience. However, it is important to emphasize that high ED alone is not sufficient to yield strong encoding performance. Indeed, it is not difficult to imagine contrived models with extremely high dimensionality but no predictive power. As a simple example, imagine a maximally sparse representation in which each stimulus elicits a response along a single, unique dimension (akin to "grandmother cells" (Barwich, 2019)). In this case, because every stimulus is represented along a unique dimension, an encoding model fit to a training set would have no ability to generalize to unseen stimuli.

In this section, we discuss some of the necessary conditions for observing a strong and positive correlation between effective dimensionality and encoding performance. In addition, we provide some empirical experiments to support our arguments.

Alignment pressure plays a significant independent role In the vocabulary of our theory laid out in Section 2.1, encoding performance depends not only on the latent dimensionality of a model, but also on its alignment pressure. And, because latent dimensionality can vary independently from alignment pressure (in the sense of independent causal interventions), it is not causally sufficient for achieving good encoding performance. Furthermore, in the infinite-dimensional space of possible visual features where model dimensions are unlikely to overlap with ecologically-relevant ones by chance, alignment pressure is essential.

In empirical models of visual cortex, the statistical relationship between alignment pressure and latent dimensionality has not been investigated. If models achieving high alignment pressure to biological representations tend to systematically have lower latent dimensionality, we might observe a net negative correlation between latent dimensionality and encoding performance. That this is not the case in our empirical results suggests that alignment pressure is probably uncorrelated (or perhaps positively) correlated with latent dimensionality.

Latent dimensionality must reflect the number of accurately-encoded features If high latent dimensionality improves encoding performance in all circumstances, we should be able to trivially obtain excellent encoding performance with any model by applying simple feature transformations. ZCA whitening, for instance, applies a linear transformation that results in a new set of features with covariance matrix close to identity (i.e., a flat eigenspectrum with maximum effective dimensionality). After applying ZCA to all models, however, we saw no improvement in encoding performance, despite significant increases in effective dimensionality, as shown in Figure J.1. Again, this shows that effective dimensionality alone is not sufficient to improve encoding performance. In this case, the reason is that ZCA whitening does not augment the model with additional information about the stimulus. Our theory in Section 2.1 states that the relationship between latent dimensionality and encoding performance depends on an assumption that higher-variance dimensions more accurately encode stimulus features. ZCA whitening, however, violates this assumption since it increases latent dimensionality by numerically scaling existing model dimensions without changing their semantics. No new dimensions are added and no existing dimensions are encoded more accurately, so encoding performance remains unchanged.

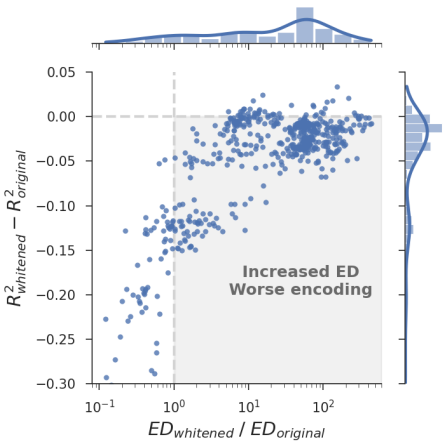

Figure J.1: Increasing latent dimensionality with ZCA whitening does not enhance encoding performance. The y-axis shows the difference in encoding performance after whitening model features, while the x-axis shows the ratio of increase in effective dimensionality. Most whitened models saw a substantial increase in effective dimensionality, but showed either no change in encoding performance or a decrease (highlighted gray region).

The empirical relationship between dimensionality and encoding performance is robust Despite the above caveats, we note that it is difficult to construct poor-performing high-dimensional models in practice, without having to resort to trivial feature transformations such as whitening. We attempted to do so by training a DNN on a version of ImageNet where the labels in the training set were randomly scrambled. Due to their large capacity, it is well known that DNNs are able to achieve low training error on this task by finding an arbitrary mapping between each input and its label, essentially memorizing the dataset (Zhang, Bengio, Hardt, Recht, & Vinyals, 2016). Our rationale for choosing this task was that it is unlikely to produce ecologically-relevant dimensions, but stands a good chance of learning a high-dimensional latent space in which it is easier to linearly separate arbitrarily labeled data (Gorban et al., 2020). However, this turned out *not* to be the case. In Figure J.2, we show the effective dimensionality and encoding

performance of a DNN fit to scrambled labels and compare it to an identical architecture fit with the correct labels. As expected, the DNN with scrambled labels achieved much lower encoding performance. Surprisingly, however, this model also had much lower effective dimensionality than its correctly trained counterpart. We speculate that ecologically-relevant visual tasks in which humans excel (and most DNNs are trained on) require high latent dimensionality as a result of their inherent complexity, producing a positive correlation between latent dimensionality and alignment pressure. We explore this possibility in Section 2.4.

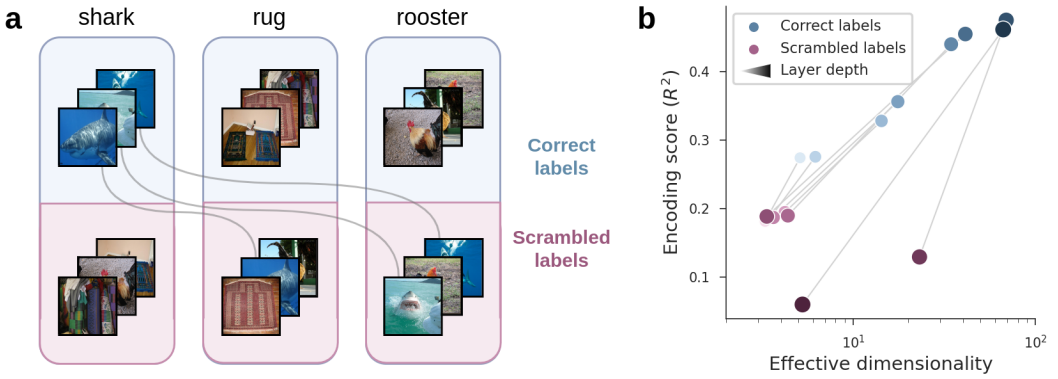

Figure J.2: Training a model to overfit scrambled labels does not increase latent dimensionality. a. We trained the same ResNet18 DNN architecture on ImageNet classification in two different settings: once with correctly labeled images (blue) and the other time with scrambled labels, such that each image was assigned to a random class. Despite the arbitrary nature of the second task, the model was able to achieve good performance on the training set (47% accuracy over 1000 classes) by memorizing an idiosyncratic mapping from each input to its label. **b.** Our initial hypothesis was that the model trained with scrambled labels would have higher effective dimensionality and lower encoding performance than the model trained with correct labels, but our results surprisingly run counter to this intuition: the model trained with scrambled labels had lower encoding performance and *lower* effective dimensionality. Blue points denote layers from the model trained with correct labels, and purple points denote layers from the model with scrambled labels. Size and brightness denote increasing layer depth, and lines indicate matching layers.